UNIVERSITAT POLITÈCNICA DE VALÈNCIA

ESCUELA TÉCNICA SUPERIOR INGENIERÍA INDUSTRIAL VALENCIA

CHEMICAL ENGINEERING MASTER THESIS

KINETIC STUDY OF THE THERMAL AND THERMO-OXIDATIVE DECOMPOSITION OF SPENT COFFEE GROUNDS UNDER INERT AND OXIDATIVE ATMOSPHERES

AUTHOR: ANTONELLA GALDO

SUPERVISOR: MARIA DESAMPARADOS RIBES GREUS

SUPERVISOR MARCO GIACINTI BASCHETTI

Academic year: 2020-21

Table of contents

Abstract 3
Keywords 3
Resumen 4
Riassunto 5
MEMORY 7
1. Motivation and aim 8
1.1. Valorisation of biomass for added value applications 8
1.2. Objectives 10
2. Introduction 11
2.1. Definition and classification of biomass 11
2.1.1. Lignocellulosic biomass 12
2.2 Biomass as a source of energy 13
2.3. Strategies for the energetic valorisation of Biomass 14
2.3.1. Pyrolysis 15
2.3.2. Combustion 16
2.4. Coffee production as a source of biomass: coffee spent grounds (CSGs) 16
2.4.1. Coffee production and characterization 16
2.4.2. Coffee production by-products 18
2.4.3. Spent coffee grounds (SCGs) 20
2.4.4. Uses of spent coffee grounds (SCGs) 24
3. Materials and methods 29
3.1. Materials 29
3.2. Thermogravimetric analysis (TGA) 30
3.2.1. Deconvolution analysis 31
3.3. Kinetic analysis of the thermal and thermo-oxidative decomposition of biomass 32
3.3.1. Calculation of the activation energy 35
3.3.2. Analysis of kinetic function 35
3.3.3. Analysis of pre-exponential factor 36
4. Results and discussion 38

4.1. Thermo-oxidative decomposition under combustion conditions 38
4.1.1. Thermo-oxidative stability 38
4.1.2. Modelling of the thermo-oxidative decomposition 42
4.1.3. Kinetic analysis of the thermo-oxidative decomposition 43
4.2. Thermal decomposition under pyrolytic conditions 49
4.2.1. Thermal stability 49
4.2.2. Modelling of the thermal decomposition 53
4.2.3. Kinetic analysis of the thermo-oxidative decomposition 54
4.3. Kinetic triplet: thermo-oxidative versus thermal decomposition 59
5. Conclusions 61
6. References 62
ECONOMIC STUDY 67
1. Detailed budget 68
1.1. Workforce 68
1.2. Equipment and tools 68
1.3. Materials and reagents 69
1.4 Supplementary costs 69
2. Total budget 70

Abstract

The growing request of energy by the global population, related to the improvement of life quality, has generated an increase of environmental pollution due to the massive use of fossil fuels. In this context, the development of new technologies may implement the use of biomass as a renewable source of energy and to generate value-added products. Particular interest has been dedicated to the lignocellulosic biomass. Coffee is one of the most popular beverages in the world and the second commodity traded after petroleum. One of his most abundant by-products is the spent coffee grounds (SCG), which contain a huge number of organic compounds that could be used for energy and added-value product generation. In this study, SCGs were examined in terms proximate analysis, ultimate analysis and calorific values and subsequently subjected to thermal and thermo-oxidative decomposition by means of thermogravimetric analysis (TGA). Thermogravimetric thermograms were obtained at different heating rates. Results were assessed by means of a deconvolution approach in order to ascertain the contribution of each component of the SCGs (hemicellulose, cellulose, lignin) to the global decomposition process. Several mathematics models were tested, and the Lorentz one was selected, approaching better the data. Finally, the kinetic triplet, constituted by the activation energy (E_a), the pre-exponential factor (A) and the model of reaction ($f(a)$), was defined through the application of iso-conversional methods, Master-Curves and Perez-Maqueda criterion. Therefore, the understanding of the thermal and kinetic parameters related to SCG may improve its thermo-chemical conversion, conducted through pyrolysis or gasification, in industrial applications.

Keywords

Thermogravimetric analysis, pyrolysis, oxidative degradation, lignocellulosic biomass, spent coffee ground.

Resumen

La creciente demanda de energía por parte de la población mundial, relacionada con la mejora de la calidad de vida, ha generado un aumento de la contaminación ambiental por el uso masivo de combustibles fósiles. En este contexto, el desarrollo de nuevas tecnologías permitirá implementar el uso de la biomasa como fuente de energía renovable y, además, generar productos de valor añadido. En este ámbito, la biomasa lignocelulósica juega un papel esencial. El café es una de las bebidas más populares del mundo y el segundo producto comercializado después del petróleo. Uno de sus subproductos más abundantes es el residuo de la preparación de bebida de café (SCG), que contiene una gran cantidad de compuestos orgánicos que podrían usarse para generar energía y otros productos de valor. En este estudio, se realizó el análisis próximo, análisis elemental y el cálculo del poder calorífico de los SCG. Posteriormente, el residuo de café fue sometido a procesos de descomposición térmica y termo-oxidativa mediante análisis termogravimétrico (TGA) a diferentes velocidades de calentamiento. Los resultados se evaluaron mediante la deconvolución de los distintos procesos para conocer la contribución de cada componente (hemicelulosa, celulosa, lignina) al proceso de descomposición global. Finalmente, se aplicaron métodos isoconversionales y curvas maestras, así como el criterio de Perez-Maqueda para obtener el triplete cinético, constituido por la energía de activación *(E_a),* el factor pre-exponencial (*A*) y el modelo de reacción (*f(α)*). La evaluación de estos los parámetros térmicos y cinéticos del SCG en la aplicación a procesos de pirólisis o gasificación puede resultar en la mejora de su conversión termoquímica, que favorezca su implantación a nivel industrial.

Palabras clave: Análisis termogravimétrico, pirólisis, degradación oxidativa, biomasa lignocelulósica, molido de café usado.

Riassunto

La crescente richiesta di energia da parte della popolazione mondiale, strettamente connessa al miglioramento della qualità della vita, ha generato un aumento dell'inquinamento ambientale dovuto all'eccessivo utilizzo di combustibili fossili. In questo scenario, lo sviluppo di nuove tecnologie fa sì che ci sia un incremento nell'utilizzo della biomassa come fonte di energia rinnovabile o per generare prodotti a valore aggiunto. Particolare interesse è stato dedicato alla biomassa lignocellulosica. Il caffè è una delle bevande più popolari al mondo e la seconda merce di scambio dopo il petrolio. Tra i suoi sottoprodotti più abbondanti troviamo i fondi di caffè esausti (SCG), contenenti un elevato numero di composti organici e potenzialmente utilizzabili per la generazione di energia e prodotti a valore aggiunto. In questo studio, gli SCG sono stati sottoposti a decomposizione termica e termo-ossidativa applicando un' analisi termogravimetrica (TGA). I termogrammi ottenuti presentano diverse velocità di riscaldamento. I risultati generati dall'analisi termogravimentrica sono stati successivamente valutati mediante un analisi di deconvoluzione, al fine di accertare il contributo di ciascun componente degli SCG (emicellulosa, cellulosa, lignina) al processo di decomposizione globale. Differenti modelli matematici sono stati testati e quello di Lorentz è stato selezionato, accostando meglio i dati fra tutti. Infine, la tripletta cinetica, costituita dall'energia di attivazione (*Ea*), dal fattore pre-esponenziale (A) e dal modello di reazione (*f*(*a*)), è stata definita mediante l'applicazione di metodi isoconversionali, Master-Curves e il criterio di Perez-Maqueda. Pertanto, lo scopo ultimo di questo lavoro prevede una migliore comprensione dei parametri termici e cinetici relativi all'SCG al fine di migliorare la sua conversione termochimica, condotta tramite pirolisi o combustione, nelle applicazioni industriali.

Parole chiave: Analisi termogravimetrica, pirolisi, degradazione ossidativa, biomassa lignocellulosica, residuo di caffè esausto

MEMORY

1. Motivation and aim

1.1. Valorisation of biomass for added value applications

Climate change, developed in recent decades, is a direct consequence of the growing demand for energy required by the population. Natural energy resources are getting depleted, while the pollution of vegetation and human health is becoming widespread. Since the energy demand is directly related to the comforts of human life, and the energy production process must be sustainable. Therefore, the development of new technologies for value-added products may offer alternatives to avoid the use of fossil fuels for energy generation and use in domestic and industrial processes.

The valorisation of biomass into value-added products requires an evaluation of feedstocks and involves its characterization, pre-treatment, or fractionation. Advice on predictive molecular modeling, on the economic assessment of the pre-treatment processes, and the valorisation strategies of biomass to value-added products, are of great importance (Daramola & Ayeni, 2020).

Several types of biomass can be employed for the generation of green products. Indeed, biomass is the oldest renewable source of energy for humans and covers a basic role in the strategic push for sustainable development (I. Dunmade, 2013). Lignocellulosic biomass (LCB) is the main type of biomass used. LCB materials are usually natural, directly available, cheap, renewable, and environmentally friendly. Their global annual production is 181.5 billion tonnes (Foukis et al., 2017). Some studies have demonstrated that LCB has enormous potential for the sustainable production of chemical substances (I. S. Dunmade et al., 2019).

The three principal components of LCB materials are cellulose, hemicellulose, and lignin. These biopolymers are interconnected in a hetero-matrix, with a variable relative composition, depending on the type, species, and origin of the material. The quantity of biomass is an essential factor to determine the final amount of energy available from the LCB materials (Isikgor & Becer, 2015). **Table 1.1** shows some of the possible pathways applied to the feedstock to obtain value-added products.

Table 1.1: Value-added processes and products (Daramola & Ayeni, 2020).

Value addition processes	Value-added products
Gasification	Methane, biohydrogen, biogas, microbial fuel cell
Biochemical conversion	Methane, biodiesel, ethanol, compost
Direct liquefaction	Methanol, liquid fuel, adhesives, biopolymers, phenolic resin, polyurethane
Pyrolysis	Bioethanol, methanol, liquid fuel, adhesives, biopolymers, phenolic resin, polyurethane, electricity
Direct Combustion	Electricity, heat

Coffee is one of the most consumed beverages in the world and spent coffee grounds (SCG) are the main coffee industry wastes. They are solid residues obtained from the treatment of coffee powder with hot water and the worldwide annual production is close to 6 million tons.

Considering the global amount of SCG produced every year, their reuse is becoming an expanding field, being the conversion into value-added products convenient from an environmental and economic point of view (Mussatto, Carneiro, et al., 2011). According to the European Landfill Directive 1999/31/EC, the disposal of SCG at landfills is discouraged in the European Union. However, it is still practiced in most developing countries around the world. Apart from the cost of landfilling, the leachate generated by SCG could deteriorate the soil and groundwater, if they are not properly collected and treated. SCG contains a high number of recalcitrant compounds, such as caffeine, tannins, and polyphenols. However, there exist some alternatives to landfilling. SCG can be used for several applications such as nutrients and antioxidant extraction, soil amendment, source of polysaccharide with immunostimulatory activity, and heavy metal absorbent, among others. Furthermore, SCG has been explored to obtain biodiesel, bioethanol, bio-ethers, bio-oil and biochar, and biogas (Tun et al., 2020).

Pyrolysis and combustion are considered among the best techniques for the thermochemical conversion of the SCG into added-value products (Basu, 2013). In this regard, the design of biomass pyrolysis and combustion facilities requires particular attention to kinetic aspects. The thermogravimetric analysis (TGA) under oxidative or inert atmospheres is a test widely used to ascertain the kinetic behaviour and the thermodynamic parameters of biomass.

In this study, the TGA was conducted with dynamic experiments involving non-isothermal multiple heating rates, leading to important information about the decomposition, such as the onset temperature (T_o), the endset temperature (T_e), and mass loss during the different decomposition steps.

Moreover, it is essential to define the kinetic model to study reactions involved in the thermochemical conversation. Indeed, the knowledge of thermal and thermo-oxidative decomposition kinetics of lignocellulosic materials permits optimizing the design of process reactors. Therefore, the assessments of the activation energy (Ea), the pre-exponential factor (A), and the kinetic function are needed (Pinzi et al., 2020).

1.2. Objectives

The main aim of this work is to study the thermal and thermo-oxidative processes of spent coffee grounds (SCG), obtained from the coffee-drink production, evaluating its suitability for future energetic valorisations. The final purpose will be achieved through the following minor objectives:

- Evaluate SCGs in terms of proximate analysis, ultimate analysis, and calorific values
- Evaluate the thermogravimetric thermograms of SCGs in terms of temperatures and mass loss in the oxidative and inert atmospheres.
- Consider the reactions occurring during the thermogravimetric analysis at multiple heating rates under inert and oxidative conditions.
- Determine and identify the decomposition processes of the different pseudo-components of the SCGs through a curve deconvolution approach.
- Estimate the activation energy to provide to SCGs pseudo-components to start the decomposition reaction under inert and oxidative atmospheres.
- Establish the decomposition mechanisms of reaction of the different components under inert and oxidative atmospheres by the use of the Master-Curves and Perez-Maqueda criteria.

2. Introduction

This chapter presents a general introduction of biomass and a detailed description of two thermochemical analyses, pyrolysis, and combustion, applied to energy enhancement. The attention is focused on the spent coffee grounds. Their production processes, characteristics, and possible valorisations are presented in detail.

2.1. Definition and classification of biomass

The definition is given by the United Nations Framework Convention on Climate Change (UNFCCC, 2005) for biomass is: "*non-fossilized and biodegradable organic material originating from plants, animals, and micro-organisms. This shall also include products, by-products, residues and waste from agriculture, forestry and related industries as well as the non-fossilized and biodegradable organic fractions of industrial and municipal wastes*" (Basu, 2013).

Biomass refers to species deriving from living or recently dead plants (botanical source) or animals (biological source), or combinations of them. It also includes gases and liquids, recovered from the decomposition of non-fossilized and biodegradable organic materials. Its composition may vary depending on age, origin, season, physical location, and other factors (Basu, 2013)(Prins, 2005).

According to the European Committee for standardization, two standards for classification, specification (EN 14961) and quality assurance (EN 15234) are used for biomass. Based on its origin, biomass is classified into four broad categories:

1. Woody biomass (trees, bushes, and shrubs).
2. Herbaceous biomass (plants that die at the end of the growing season).
3. Fruit biomass.
4. Blend and mixtures (the first are intentional mixing of biomass, while mixtures are unintentional mixing of biomass).

Another classification is made between primary biomass and waste biomass:

- Primary or virgin biomass comes directly from plants or animals and includes wood, plants, and leaves (lignocellulose), crops and vegetables (carbohydrates), etc.
- Waste or derived biomass comes from different biomass-derived products and includes solid (municipal solid waste), liquid (sewage, animal, and human waste), and gases (landfilling) wastes (Basu, 2013).

Therefore, the main sources of biomass are:

- Agricultural: food grain, bagasse (crushed sugarcane), corn stalks, straw, seed hulls, nutshells, and manure from cattle, poultry, and hogs.
- Forest: trees, wood waste, wood or bark, sawdust (SW), timber slash, and mill scrap.
- Municipal: sewage sludge, refuse-derived fuel (RDF), food waste, waste paper, and yard clippings.
- Energy Crops: poplars, willows, switchgrass, alfalfa, prairie bluestem, corn, and soybean, canola, and other plant oils.
- Biological: animal waste, aquatic species, and biological waste.

2.1.1. Lignocellulosic biomass

Biomass is a complex mixture of organic materials, such as carbohydrates, fats, and proteins, with small amounts of minerals composed of sodium, phosphorus, calcium, and iron. Focusing on the woody biomass, extractives, fiber or cell wall components, and ash are the main components. More in detail, the cell wall is composed of lignin, cellulose, and hemicellulose. For this reason, it is also defined as lignocellulosic biomass. A lignocellulosic material corresponds to the fibrous and non-starchy part of plant materials. Unlike starch and carbohydrates, lignocellulose is not easily digested by humans, so it is not part of the food chain, and its use as a source for the generation of energy does not affect the world's food supply (Basu, 2013).

Cellulose is a glucose polymer consisting of repeating units of $C_6H_{10}O_5$ linked together through β-glycosidic bonds. The β bonds form linear chains, that are highly stable and resistant to chemical attack due to the high degree of hydrogen bonding, that can occur between the cellulose chains. The hydrogen bond makes the polymers rigid, inhibiting the bending of the molecules, which must occur in the hydrolytic breakdown of the glycosidic bonds. Hydrolysis can reduce cellulose to a repeating unit of cellobiose, $C_{12}H_{22}O_{11}$, and finally to glucose, $C_6H_{12}O_6$. It is also the main constituent of wood and represents the structural reinforcement of the wooden cells (Hornung, 2014).

Hemicellulose is a short, highly branched sugar chain. It's a polymer made up of five different sugars, including sugars with five carbon atoms (usually D-xylose and L-arabinose), sugars with six carbon atoms (D-galactose, D-glucose, and D-mannose), and uronic acid. The sugars contain a high percentage of acetic acid as a substituent. Due to the branched nature, hemicellulose possesses amorphous properties. Thanks to its sugars, it is easily hydrolysable compared to cellulose. When hydrolysed, hemicellulose releases products with a high content of xylose (a five-carbon sugar) (Hornung, 2014).

Lignin is the main non-carbohydrate polyphenolic structural constituent of wood. Its role is to encrust the cell walls and allow the cells to be cemented together. It is a highly polymeric substance, with a complex, cross-linked, aromatic structure and with a molecular weight of approximately 10.000. It's mainly derived from coniferyl alcohol ($C_{10}H_{12}O_3$) by extensive condensation and polymerization (Hornung, 2014).

Figure 2.1. shows the structure and the basic components of lignocellulosic biomass and **Table 2.1** give the organic components of some of the energy crops, common sugar, and starch crops, respectively.

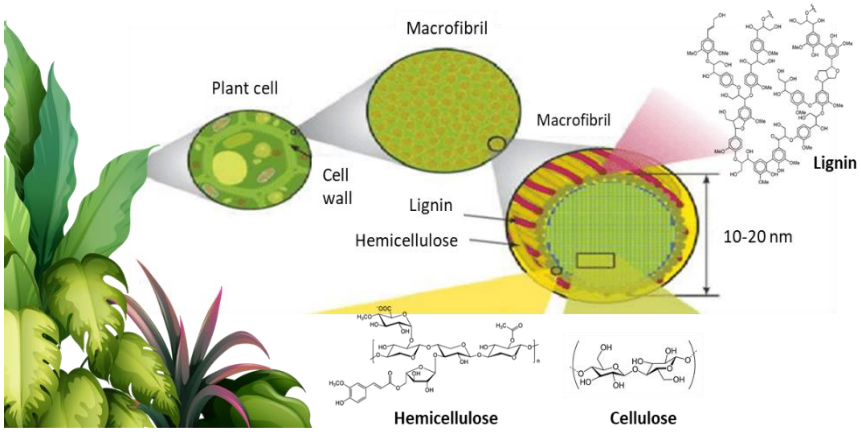

Figure 2.1: Basic components of lignocellulosic materials.

Table 2.1: Organic components and composition of lignocelluloses biomass (Hornung, 2014).

Feedstock	Cellulose (wt.%)	Hemicellulose (wt.%)	Lignin (wt.%)	Other (wt.%)
Bagasse	35	25	20	20
Bamboo	55	28	17	0
Corn stove	53	15	16	16
Corncob	32	44	13	11
Herbaceous energy crops	45	30	15	10
Rice straw	38	25	12	25
Short rotation woody crops	50	23	22	5
Wheat straw	38	36	16	10
Wheat chaff	38	36	16	11
Waste paper	76	13	11	0

2.2 Biomass as a source of energy

Over the past twenty years, the European Union (EU) has worked to ensure that all member states implement a comprehensive and coherent policy aimed at reducing global pollution and dependence on external energy sources. The main goals of this policy are: (*i*) the reduction of energy consumption; (*ii*) greater use of renewable sources; (*iii*) diversification of energy sources; and (*iv*) increase in international cooperation for energy trade. In this regard, the use of more renewable sources could lead to an improvement not only of the environment but also of competitiveness. It was also noted that bioenergy can generate many other types of benefits such as the promotion of regional economic structures, an alternative source of income for farmers, etc (McKendry, 2002). The biomass contribution to primary energy production presents a reasonable cost-benefit use, and a series of measures are aimed at increasing its use, by creating market incentives and eliminating obstacles to its development (McKendry, 2002).

In the last decade, there has been a growing interest in biomass as a source of energy and it is currently estimated to account for 10-14 % of the world supply. Numerous economic studies have shown that increasing biomass use has several key benefits, achieved without increasing pollution or other damage to the environment. The use of agricultural waste and food surpluses as biomass for energy obtaining may achieve greater conversion efficiency at lower costs. The cost of energy produced from biomass is already competitive concerning that produced using fossil fuels. Moreover, due to the threat posed by climate change, linked to the high release of greenhouse gases, particular attention is given to the use of renewable resources such as biomass. Indeed, it has been observed that sustainably produced biomass emits approximately the same amount of carbon that is able to absorb during plant growth. Hence, the use of biomass does not contribute to the accumulation of CO_2 in the atmosphere (McKendry, 2002). Biomass production also generates jobs (250.000 to 300.000 direct jobs in Europe every year, mainly in rural areas) and the replacement of intensive agriculture with less energy-

intensive crops can be achieved with environmental benefits, such as reduced fertilizer leaching and reduced use of pesticides. Furthermore, if appropriate crops are selected, restoration of degraded soils may be possible. Finally, the diversification of energy supply in the last years has generated a potential pressure point towards a reduction in the price of oil as a result of a decrease in demand (McKendry, 2002) (Nunes et al., 2018). In addition, when available, the use of biomass can avoid this traditional fuel dependence in undeveloped countries.

2.3. Strategies for the energetic valorisation of Biomass

Generally, in a thermochemical conversion process, the entire biomass is converted into gas. It is subsequently synthesized into the desired chemicals or used directly, as schematised in **Figure 2.2**. Five different paths can be followed to obtain the production of thermal energy: (*i*) combustion; (*ii*) carbonization/roasting; (*iii*) pyrolysis; (*iv*) gasification; and (*v*) liquefaction.

Combustion involves high-temperature exothermic oxidation in hot fumes in presence of an oxygen-rich environment. Carbonization, instead, involves the increase of carbon content in organic materials through chemical decomposition. In this process, the production of carbon from biomass is obtained in an oxygen-free atmosphere and with very slow heating up to the carbonization temperature (about 500 °C). In roasting, the biomass is heated up to a lower temperature of 200-300 °C, in an almost oxygen-free environment. Pyrolysis, on the other hand, involves rapid or slow heating in the total absence of oxygen. Gasification involves chemical reactions in an oxygen-deficient environment. The final product consists of gases with different heating values. Finally, in liquefaction are obtained liquids characterized by low molecular weight molecules, starting from solids characterised by high molecular weight molecules. It occurs in the presence of a catalyst and at low temperatures (Basu, 2013).

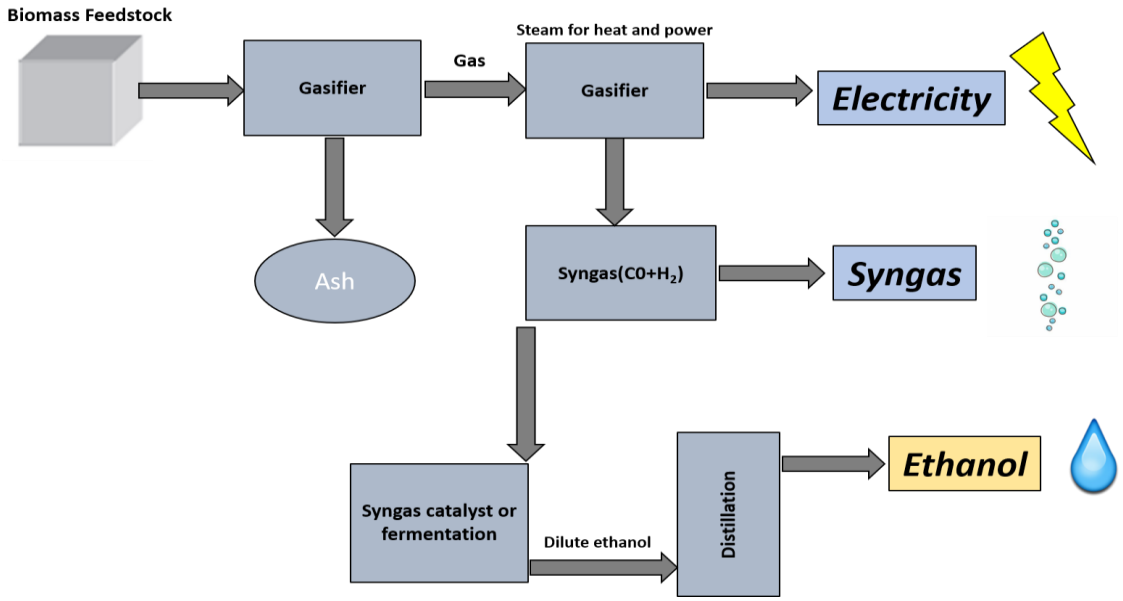

Figure 2.2: Thermochemical route for the production of energy, gas, and ethanol (Basu, 2013).

The attention is focused on the pyrolysis and combustion processes, as they are considered some of the most promising processes for the conversion of lignocellulosic biomass into energy.

2.3.1. Pyrolysis

Pyrolysis generally takes place in environments with a total absence of oxygen, except for cases where partial combustion may supply the thermal energy necessary for the process. Indeed, pure pyrolysis is a non-exothermic conversion process (Basu, 2013)(Primaz, 2018)(Yaman, 2004)(Mohan et al., 2006). It involves the thermal decomposition of biomass into gas, liquid, and solid, through heating above 300-400 °C. Particularly, during the pyrolysis of biomass, hemicellulose is degraded at temperatures between 225 and 325 °C, cellulose between 305 and 375 °C, and lignin between 250 and 500 °C (Basu, 2013). Pyrolytic reactions involve chain breakages and molecular weight reduction, but also re-combinations of chemical bonds, to form new compounds that can be used as fuels or chemical inputs. From this process three different reaction products are obtained which are:

1. Pyrolytic gas (volatile matter): composed mainly of carbon monoxide (CO), carbon dioxide (CO_2), hydrogen (H_2), light hydrocarbons, traces of some larger organic components, and water vapor.
2. Bio-oil: a dark-colored liquid, which originates from condensable organic vapours.
3. Biochar: a solid commonly called biochar, which is rich in carbon and not volatilises.

The solid and liquid products of the first stage can react again (degradation reactions in the condensed phase), giving way to more volatile compounds, or they can polymerize or poly-condensate, generating a new liquid or solid phase. In the second phase, the volatile species undergo more heterogeneous reactions with solids residues or homogeneous reactions in the gas phase. The heat added to the inert atmosphere causes the breaking of the C-C bonds of the organic components of the biomass, forming CO bonds. Redox reactions also occur, in which part of the biomass is reduced to carbon and another part is oxidized and hydrolysed, giving rise to phenols, carbohydrates, alcohols, aldehydes, ketones, and carboxylic acids. The yield and properties of the products depend on the nature of the raw material, type of reactor, and the operating conditions (temperature, heating rate, vapor residence time, type, and quantity of catalyst). Concretely considering the operating conditions, if the pyrolysis temperature increases, the yield of bio-oil and gaseous product increases, but the yield of biochar is reduced. For the heating rate, generally the higher the rate, the greater the yield of bio-oil, even if the latter contains a high percentage of highly reactive oxygenated compounds, with characteristics that can change rapidly during condensation.

According to the heating rate of the pyrolysis, it may be classified as:

- Slow pyrolysis: the biomass is pyrolyzed at slow heating rates (0.1 -1 $\frac{^{\circ}C}{min}$). The main type of product is biochar. The temperature reached is generally from 300 to 700 °C. The size of the particles used is between 5 and 50 mm and the residence time of the solids inside the reactor is between 600 and 6000 s.
- Rapid Pyrolysis: the biomass is heated rapidly (up to 100 $\frac{^{\circ}C}{min}$), reaching high temperatures (600 - 1000 °C). The main type of product is bio-oil. The particle size used is less than 1 mm and the residence time of the solid is between 0.5 and 5 min.
- Flash pyrolysis: the reaction time is only a few seconds or less. The heating rate is very high (1000 $\frac{^{\circ}C}{min}$ or higher). Due to the high heating rate, the particle size must be very small, i.e. less than 0.5 mm.

2.3.2. Combustion

Combustion is an exothermic chemical reaction, that takes place between the fuel and an oxidant, which can be air or pure oxygen, accompanied by the production of heat and conversion of chemical species. In a complete combustion reaction, fuel reacts with the oxidising element, and the products are oxidised compounds of each pseudo-component of a given fuel, such as biomass. During the global process, competitive reactions occur ascribed to sub-processes like drying and/or pyrolysis.

Biomass can be used as a stand-alone fuel or as a supplement to fossil fuels for combustion processes. Among them, the combination with other fuels is becoming increasingly popular to reduce the generation of pollution and neat CO_2 in fossil fuel plants.

Equation 2.1 shows a general combustion reaction:

$$C + O_2 \rightarrow CO_2 \qquad \textbf{(2.1)}$$

When 1 k mol of carbon is completely burnt in air or oxygen, it produces carbon dioxide and approximately 394 $\frac{kJ}{kmol}$ of heat.

Heat and electricity are two principal forms of energy derived from the combustion of biomass. The heat released from combustion constitutes the largest source of human energy consumption. When produced, it can generate the formation of light, in form of glowing or luminous flame. In rural areas, this heat is used for cooking and warmth. Also, industrial heating is produced by steam generated in biomass-fired boilers. For the production of electricity, the usual practice involves the creation of steam by burning biomass in a boiler and the generation of electricity through a steam turbine. Therefore, this thermochemical process has as final aim the conversation of energy contained in the fuel into sensible heat, transferring the chemical energy in the fuel to the product of combustion (Basu, 2013) (Hornung, 2014).

2.4. Coffee production as a source of biomass: coffee spent grounds (CSGs)

2.4.1. Coffee production and characterization

Worldwide, coffee is the second-largest commodity after petroleum. World coffee production is estimated to have grown by 10% from 1950 to 1960 and more than 0.5–1.9% until 2010. Production locations are currently spread all over the world. However, the ten largest coffee-producing countries are responsible for around 80% of world production (South America with around 43%, Asia with 24%, Central America with 18%, and Africa with 16%). Brazil, Vietnam, Colombia, and Indonesia are respectively the first, second, and third world producers, responsible for more than half of the world's supply of coffee. In 2005, global coffee production was estimated at around 124.636 million of 60 kg bags. Despite the financial crisis, the world consumption of coffee in 2008 was around 128 million bags, while in 2017 it had increased to around 160 million of 60 kg bags (Mussatto, Machado, et al., 2011)(Tun et al., 2020).

Among the various species of Rubiaceae coffee, the most used for coffee production, those that have international relevance in terms of business volume are the Arabica and Robusta varieties, of which the first is particularly valuable and reaches very high prices in export. It corresponds to the seed of the natural coffee plant and is thought to have been first grown in Ethiopia.

The coffee cherry is the raw fruit of the plant and consists of two hemispherical seeds with flat and contact front sides, covered with a thin shell-like parchment and further surrounded by the pulp. These cherries are usually harvested after five years of planting coffee trees and when the fruit turns green to red (Mussatto, Machado, et al., 2011). **Figure 2.4** shows a schematic plot of the longitudinal cross-section of the coffee cherry.

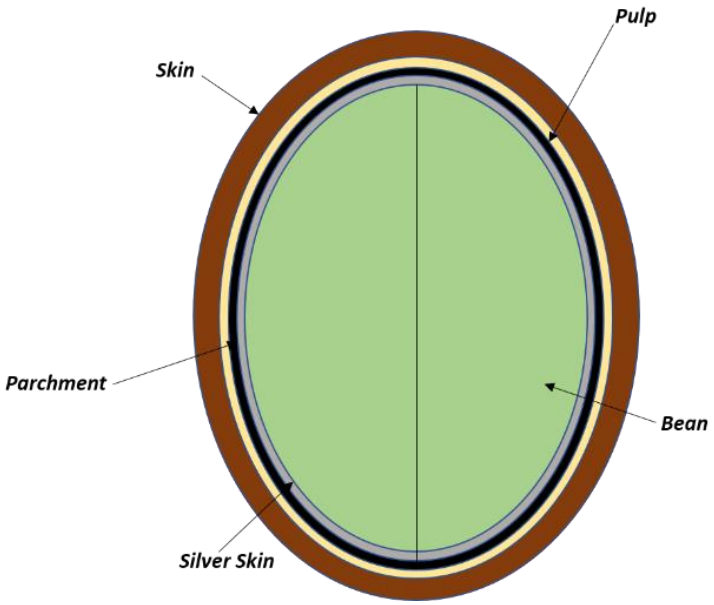

Figure 2.4: Longitudinal cross-section of the coffee cherry (Mussatto, Machado, et al., 2011).

The main constituent of the coffee seed is the endosperm, which contains high amounts of caffeine, a substance that takes its name from the coffee seed. Thanks to this substance, which gives coffee stimulating and sensory properties, its commercial relevance has reached a very high level, and it is currently one of the most exported products in the world (Mussatto, Machado, et al., 2011). In the raw Arabica coffee, caffeine can be found in values varying between 0.8% and 1.4%, while for the Robusta variety these values vary between 1.7% and 4.0%. Moreover, the coffee drink contains various components responsible for the biological and functional effects, such as the prevention of diseases and the maintenance of good health, and some of them possess nutraceutical effects (Primaz, 2018)(Bedmutha et al., 2011)(Mussatto, Carneiro, et al., 2011).

Coffee processing begins with the conversion of coffee cherries into green coffee beans. The first step corresponds to the removal of the pulp or the peel, using a wet or dry method. Depending on the processing approach of the coffee cherries, the solid residues obtained have one of the two names (pulp or peel). The dry method is generally used for Robusta and from a technological point of view it is more radical and intuitive than the wet method, generally used for Arabica coffee beans (Mussatto, Machado, et al., 2011).

The roasting of the coffee beans is the second step. It's a fundamental stage in the processing of coffee as it brings specific organoleptic properties (flavours, aromas, colour), that influence the quality of the coffee. This process depends on time and temperature and leads to various changes in the chemical composition and biological activities of the coffee. It is very important to remember that after roasting

the coffee beans must be cooled quickly to avoid the formation of exothermic reactions and excessive roasting, which could compromise the quality of the product.

Finally, the roasted beans are ground, usually using a multistage coffee grinder, vacuum-sealed, and shipped. For the production of instant coffee, it is necessary to add a further extraction step. The soluble solids and volatile compounds, that provide aroma and flavour, are extracted from the coffee beans, using water heated to approximately 175 °C under pressurized conditions (Mussatto, Machado, et al., 2011).

2.4.2. Coffee production by-products

The food and agri-food sectors generate a very high quantity of both liquid and solid residues. Given the widespread production of coffee, a very high amount of waste is generated. Between the years 1930 and 1943, 77 million bags of green coffee were burnt or landfilled, in the absence of any type of law for their disposal. In recent years these products have become a field of study. Considering that more than 50% of the coffee fruit is not used for the production of coffee, it is discarded during processing. It is currently interesting to find applications for these by-products. Particularly, coffee silver-skin (CS) and spent coffee grounds (SCG) are the main residues of the coffee industry. Until now, the great part of the applications has been in industries different from the food industry, such as power generation, adsorption of compounds, and manufacturing of industrial products (particleboard, ethanol, gibberellic acid, and α-amylase).

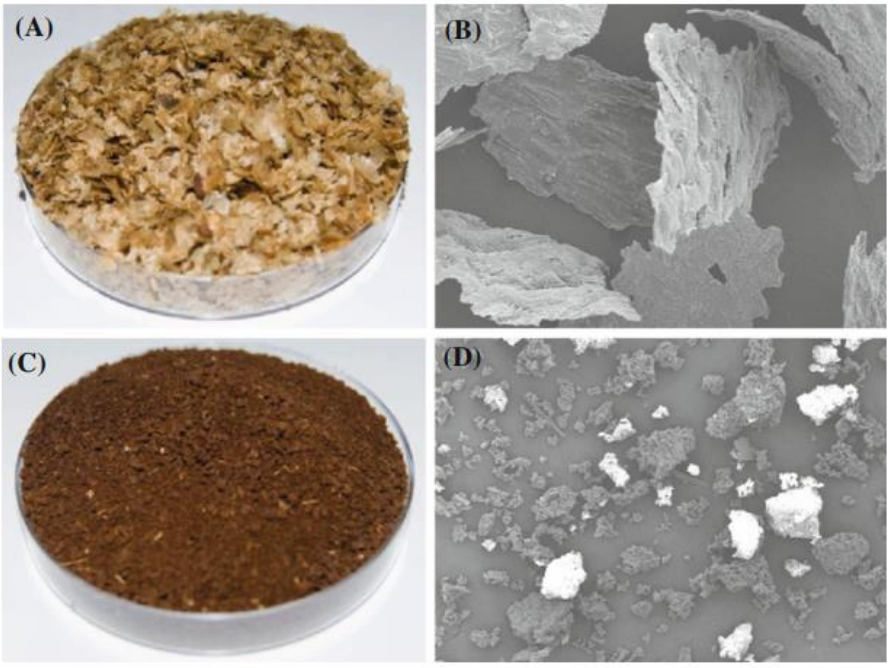

Figure 2.5: Appearance of coffee silver-skin (a, b) and spent coffee grounds (c, d). Scanning electron microscopy (b, d) of particles at 50-fold magnification (Mussatto, Machado, et al., 2011).

Coffee silver-skin (CS) is a coffee bean integument obtained as a by-product of the roasting process. Its remnants, still attached to the green coffee beans, are removed during this process. It corresponds to a residue with a high concentration of soluble dietary fiber (86% of the total dietary fiber) and a high

antioxidant capacity, due to the low concentration of phenolic compounds (**Table 2.2**). Microscopic examination (**Figure 2.5**) highlights the presence of fibrous tissues from the superficial layers, containing cellulose and hemicellulose. As for the monosaccharides, it's possible to find glucose, xylose, galactose, mannose, and arabinose. Proteins and extractives are also present in significant fractions. It is recommended his use as a functional ingredient and also it is important to underline that it supports the growth of bifid-bacteria *in vitro*, which might have some beneficial effects.

Table 2.2: Chemical composition (g/100 g) of coffee silver-skin (CS) and spent coffee grounds (SCG) (Mussatto, Machado, et al., 2011).

Components	CS	SCG		
	A	B	C	D
Cellulose (glucose)	N. d.	17.8	8.6	N. d.
Hemicellulose	N. d.	13.1	36.7	N. d.
Xylose	N. d.	4.7	0.0	N. d.
Arabinose	N. d.	2.0	1.7	N. d.
Galactose	N. d.	3.8	13.8	N. d.
Mannose	N. d.	2.6	21.2	N. d.
Protein	18.6	16.2	13.6	N. d.
Fat	2.2	N. d.	N. d.	N. d.
Ashes	7.0	4.7	1.6	N. d.
Extractives	N. d.	15.0	N. d.	N. d.
Total Fibres	62.4	N. d.	N. d.	N. d.
Soluble	53.7	N. d.	N. d.	N. d.
Insoluble	8.8	N. d.	N. d.	N. d.
Organic matter	N. d.	N. d.	N. d.	90.5
Nitrogen	N. d.	N. d.	N. d.	2.3
Carbon/Nitrogen (C/N ratio)	N. d.	N. d.	N. d.	22/1

Spent coffee grounds (SCGs) are a residue characterized by fine particle size, a high percentage of humidity (between 80% and 85%), organic load, and acidity. The latter results from the treatment of raw coffee powder with hot water or steam for the preparation of soluble coffee. Almost 50% of world coffee production is used for the preparation of soluble coffee. Numerically, 1 ton of green coffee generates about 650 kg of SCG, and about 2 kg of wet SCG are obtained for every 1 kg of soluble coffee produced.

Complementarily, other types of by-products are generated during coffee production. As well, low-quality coffee, containing spots, black or dark brown unripe fruit, or other kinds of imperfections are usually discarded and constitutes about 15-20% of world production.

Coffee husks are made up of the outer skin of the coffee berry, pulp, and parchment. They are products of dry coffee processing and are rich in carbohydrates (35%), proteins (5.2%), fibers (30.8%) and mineral salts (10.7%) The skin and pulp of coffee have a similar composition to that of the husks, i.e. proteins (7.5-15.0%), fats (2.0-7.0%) and carbohydrates (21-32%). It is not possible to use these by-products for animal food due to the anti-physiological and anti-nutritional factors present. However, the husk, skin, and pulp of coffee can be a source of phytochemicals for the food and pharmaceutical industries (Esquivel & Jiménez, 2012).

Mucilage is composed of water (84.2%), proteins (8.9%), sugar (4.1%), pectic substances (0.91%) and ash (0.7%). Pectic substances contain uronic acids (60%) with a high degree of methyl esterification and a moderate degree of acetylation. In the wet coffee processing process, and in particular, after purification without enzymatic degradation, the mucilage fraction remains adherent to the coffee bean.

Parchment is the strong fibrous endocarp that covers both hemispheres of coffee and separates them from each other. It consists of (α-)cellulose (40–49%), hemicellulose (25–32%), lignin (33–35%), and ash (0.5–1%). In the dry processing process, the parchment is separated from the green coffee beans with the skin and pulp, in a single step. However, to exploit only this product, separately from the other by-products, it's necessary to carry out wet processing, in which the parchment is removed, after drying and peeling, in separate phases.

Products derived from the extraction and concentration of water-soluble products, which could generate environmental problems; have received great attention to research methods of reuse. Indeed, it was found that these could be a source of bio-actives. Their extracts are a biological source with strong anti-radical, antioxidant, antitumor activity, and a limited anti-inflammatory and anti-allergic action (Esquivel & Jiménez, 2012).

2.4.3. Spent coffee grounds (SCGs)

Chemical composition

As mentioned in the previous section, SCGs are one of the main by-products in coffee production. On average, 1 g of ground coffee produces 0.91 g of spent grounds. Spent coffee grounds contain large amounts of organic compounds such as fatty acids, lignin, cellulose, hemicellulose, and other polysaccharides and other elements (minerals) that can be exploited as a source of value-added products, as shown in **Figure 2.6**.

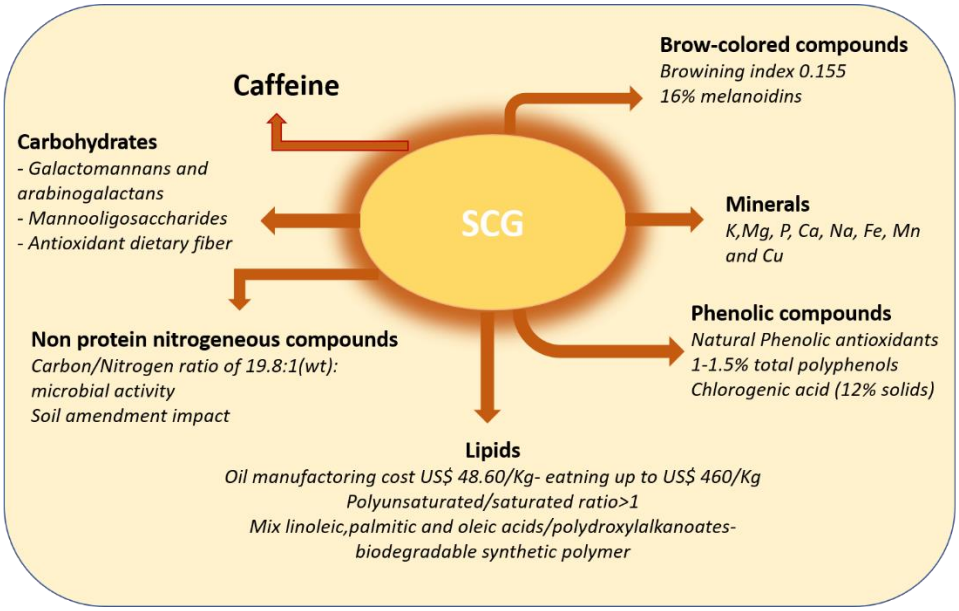

Figure 2.6: Value-added products/sustainability of the coffee agroindustry (Campos-Vega et al., 2015)

Based on the dry weight, 65% of SCG is composed of hemicellulose and cellulose. Minerals include potassium, magnesium, calcium, sodium, iron, manganese, rubidium, zinc, copper, strontium, chromium, vanadium, barium, nickel, cobalt, lead, molybdenum, titanium, and cadmium. Among the sugars, sucrose, glucose, fructose, arabinose, galactose, and mannose are present. Due to the high content of simple carbohydrates, the metabolic activation of this product is very simple and this leads to an increase in the growth of putrescible microorganisms, such as molds. Several amino acids, such as alanine, arginine, asparagine, cysteine, glutamic acid, glycine, histidine, isoleucine, leucine, lysine, methionine, phenylalanine, proline, serine, threonine, tyrosine, and valine can also be found inside them. Of all the substances present, only caffeine is thermostable, due to its capacity to be not destroyed by excessive roasting. Other substances such as proteins, sugars, chlorogenic acid, trigonelline, and fat can be destroyed and transformed into reactive products during the coffee roasting process (Esquivel & Jiménez, 2012)(Bedmutha et al., 2011).

Regarding the chemical composition, **Table 2.3** shows the results gathered from different studies in the literature (Ballesteros et al., 2014) (Stylianou et al., 2018) (Murthy et al., 2009)(Mussatto, Machado, et al., 2011)(Obruca et al., 2015) (Lee et al., 2021)**.**

The most abundant component in the SCG is polysaccharides. The sugars are polymerized into cellulose and hemicellulose structures and in total correspond to around 50% of the composition by dry weight. In absolute, hemicellulose is the most abundant component. It is composed of 37.03% mannose, 31.90% galactose, 24.08% glucose, and 6.99% arabinose. The percentages of sugars are not fixed and some differences could be attributed to the extraction process and the variety of coffee beans used. Lignin, on the other hand, has a percentage of approximately 25%. It is a macromolecule composed of several functional groups including phenolic hydroxyl, aliphatic hydroxyl, methoxy, carbonyl, and sulfonate. Its main acids present are chlorogenic, caffeic, and coumaric acid. Particular interest is devoted to these elements for their antioxidant properties (Stylianou et al., 2018)(Ballesteros et al., 2014). The ash level of the SCG is 1.30%. Among the minerals present, it is

possible to find potassium, calcium, magnesium, sulphur, phosphorus, iron, manganese, boron, copper, and others (**Table 2.4**). Potassium is the most abundant element, followed by magnesium and phosphorus. They are considered essential micronutrients for humans, due to their ability to regulate hormonal and enzymatic activities, electrolyte balance, and normal growth or vital processes, such as breathing, digestion, and circulation. SCG residues are rich in polysaccharides, lignin, proteins, and minerals, showing their high biotechnological value.

Table 2.3: Composition of SCGs.

Component	**Content (wt%)**		
	(Ballesteros et al., 2014).	(Stylianou et al., 2018) (Murthy et al., 2009)(Mussatto, Machado, et al., 2011)(Obruca et al., 2015)	(Lee et al., 2021)
Cellulose (glucose)	12.40 ± 0.79	8.6-13.3	16.78
Hemicellulose	39.20 ± 1.94	30-40	48.22
Proteins	17.44 ± 0.10	6.7-13.6	19.42
Oil	2.29 ± 0.30	10-20	
Lignin	23.90 ± 1.70	25-33	34.94
Insoluble	17.59 ± 1.56		
Soluble	6.31 ± 0.37		
Polyphenols		2.5	N. d.
Caffeine		0.02	N. d.
Arabinose	3.60 ± 0.52	1.7	N. d.
Galactose	16.43 ± 1.66	13.8	N. d.
Mannose	19.07 ± 0.85	21.2	N. d.
Ashes	1.30 ± 0.10	1.6	N. d.
Organic matter	60.46 ± 2.19	90.5	N. d.
Nitrogen	2.79 ± 0.10	2.3	N. d.
Carbon/nitrogen (C/N ratio)	16.91 ± 0.10	22/1	N. d.

Table 2.4 : Mineral composition of SCGs (Ballesteros et al., 2014).

Mineral Elements	Composition (mg/Kg dry material)
Potassium	11,700 ± 0.01
Calcium	1,200 ±0 .00
Magnesium	1,900 ± 0.00
Sulphur	1,600 ± 0.00
Phosphorus	1,800 ± 0.00
Iron	52.00 ± 0.50
Aluminium	22.30 ± 3.50
Strontium	5.90 ± 0.00
Barium	3.46 ± 0.05
Copper	18.66 ± 0.94
Sodium	33.70 ± 8.75
Manganese	28.80 ± 0.70
Boron	8.40 ± 1.10
Zinc	8.40 ± 0.20
Cobalt	15.18 ± 0.05
Iodine	<0.10
Nickel	1.23 ± 0.59
Chromium	<0.54
Molybdenum	<0.08
Vanadium	<0.29
Lead	<1.60
Selenium	<1.60
Gallium	<1.47
Tin	<1.30
Cadmium	<0.15

Functional Properties

The water holding capacity (WHC) corresponds to the ability of a material to retain water inside it, following the application of a centrifugal or compressive force, while the oil holding capacity (OHC) is closely related to the oil. As shown in **Table 2.5**, both parameters have high values for SCG and according to some authors they could be related to particle size. It has been scientifically tested that a material with a higher packing density value, due to the smaller size of its particles, has higher values of WHC and OHC. However, the nature and structure of the particles can also influence the distribution of oil and water (Ballesteros et al., 2014).

The other two properties are the emulsifying activity (EA), which represents the ability of a material to form a homogeneous dispersion of two immiscible liquids or emulsions, and the emulsifying stability (ES), which is the effectiveness of a molecule to maintain a thermodynamically stable emulsion. The values relating to the SCG are all present in **Table 2.5** and show that this material has excellent emulsifying capacities, both in terms of activity and stability, and it is used as an emulsifier in various foodstuffs, for both humans and animals (Ballesteros et al., 2014).

Table 2.5: Functional and physiological properties of spent coffee grounds(Ballesteros et al., 2014).

Functional and physiological properties	SCG
WHC (g water/g dry sample)	5.73 ± 0.10
OHC (g oil/g dry sample)	5.20 ± 0.30
Emulsifying activity (%)	54.72 ± 0.90
Emulsion stability (%)	92.38 ± 0.90

2.4.4. Uses of spent coffee grounds (SCGs)

Nowadays, one of the main problems related to the production process concerns the disposal of waste, especially related to the agricultural and food industry. Apart from the high cost of landfilling, the product from SCG deteriorates the quality of the soil and groundwater, if not properly collected and treated, because they contain a series of recalcitrant compounds, such as caffeine, tannins, and polyphenols. The introduction of a circular economy and the hierarchy developed by the European Union currently obliges producers to search for new strategies for the disposal of their waste.

The principle of the circular economy provides that the wastes of different types of industrial processes are reused as raw materials for new processes. For this, it is necessary to reconcile different technologies to reduce waste production, increase valuable resources for different applications and allow the generation of new improved products. (Mata et al., 2018). The SCG corresponds to a set of organic wastes, which can be used as an additive in various processes. This application is a perfect representation of the concept of circular economy, because guarantees the reduction of the number of wastes, generating economic benefits, and decreases the environmental impact.

One of the main challenges of the last decade is the coverage of the waste collection system. It is currently regulated by various parameters such as the population density, product volume, interest in participating, collection services available, energy consumption over transport distances, and fuel consumption rates or dispersion of SCG sources. The latter parameter is particularly important when

the object of interest corresponds to a small country. Until five years ago, the SCGs have been mainly commercially used for the production of mushrooms and coffee strains, biomass pellets, biodiesel, or biochemicals as summarised in **Table 2.6**. In the last years, several new projects, related to different fields, have been developed. For example, in November 2017, in London was launched an initiative for red buses. Particularly, the SCG was used to produce coffee biofuels, through a collaborative project of Bio-bean Ltd. with Royal Dutch Shell Plc (Stylianou et al., 2018).

Table 2.6: Market products from SCGs (Stylianou et al., 2018).

Company	Country	Products
Bio-bean	UK, London	Coffee logs, biomass pellets, biodiesel, and biochemicals
LifeCykel	Australia, Melbourne	Mushrooms
Recyworks	Greece, Athens	Mushrooms
GroCycle Urban Mushroom Farm	UK, Devon	Mushrooms
Green Cup Ltd.; re-worked furniture	UK, London	Garden products (soil conditioners) and Çurface for furniture (Çurface is a special material made for interior surfaces and panels)
Blanc de Gris	Canada, Montreal	Mushrooms
Pine Mountain Hearthmark	USA	Java log

Moreover, thanks to all the substances of which SCGs are composed, they can be reused in the agricultural and food fields. Although the high lignin content may prevent its direct application in the food industry, it has been demonstrated that with the improvement of extraction methods, the obtained bioactive compounds can be used in the pharmaceutical industry (Stylianou et al., 2018). An overview of potential uses is shown in **Figure 2.7**. Then, some of the most extended uses are described in detail.

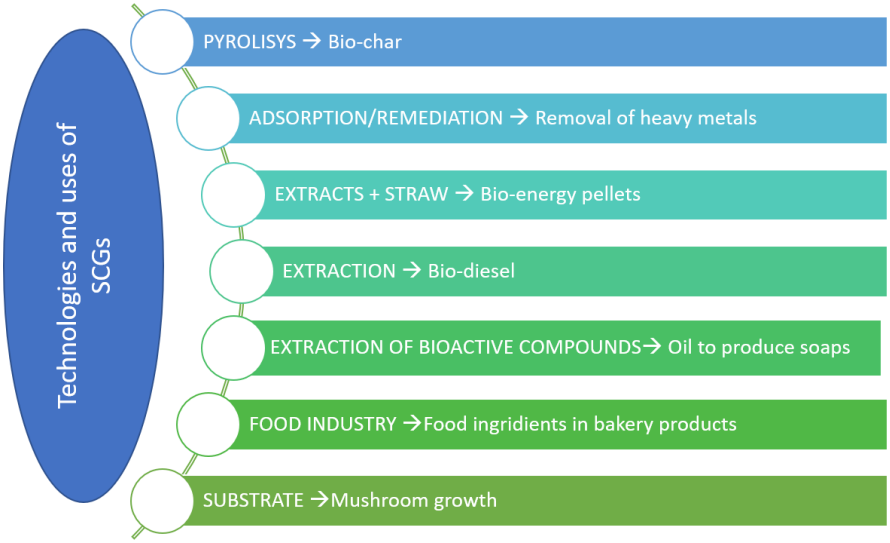

Figure 2.7: Overview of some potential usages of SCG.

Source of natural anti-oxidants

,To recover phenolic compounds, which can act as food supplements or can be exploited in the medical and pharmaceutical fields, the antioxidant power of SCG has been studied (Mussatto, Ballesteros, et al., 2011). SCGs are rich in natural antioxidants (chlorogenic acids and trigonelline), and other elements obtained during roasting (melanoidins and nicotinic acid). Phenolic compounds are generally used in the medical field, thanks to their protective action against chronic degenerative diseases (macular degeneration, neurodegenerative diseases, and diabetes mellitus), cardiovascular diseases, anticancer and antiallergic activities.

The total phenolic content of SCG is expressed as gallic acid equivalents (GAE) and has a range from 17 to 35 $mg \cdot g^{-1}$ dry waste, while agro-industrial waste has a value <15 $mg \cdot g^{-1}$ dry matter. Indeed, different studies have been conducted to examine extraction methods of the phenolic compounds, such as alkaline, saline, and acids (Stylianou et al., 2018).

Agronomic potential of SCG

In recent years, one of the problems that have most influenced the field of cultivation is related to the use of fertilizers and the environmental impact that they can cause. It has been observed that the use of SCG as a fertilizer can represent a promising alternative to standard chemical fertilizers, reducing the environmental impact and generating a promising source of nutrients, which can improve soil structure, aeration, and fertility. It is important to specify that some negative effects have been observed. One of these could be the incorporation of crude SCG into the soil. The responses of plants, can be different depending on the plant species and the quantity of SCG introduced. Negative effects are attributed to phytotoxic (Yamane et al., 2014) and oxidative effects. It happens because the SCG is rich in polyphenol compounds, characterized by phytotoxic properties (C. Santos et al., 2017). It has been discovered that one of the reduction techniques of these compounds can be constituted by composting because during this process the high microbial activity and temperature increase the degradation of the great part of polyphenolic compounds (Volf et al., 2014)(Stylianou et al., 2018).

SCG as a recycled construction material

In recent decades, the SCG has been evaluated as a reinforcing material in the construction sector. Its main use is related to the foundations of solid embankments. Several environmental and engineering tests have been carried out on this material to verify its properties. Low concentrations of heavy metals (As, Cd, Cr, Cu, Hg, Ni, Zn), cyanide, and polycyclic aromatic compounds have been detected. In addition, a high organic content, low maximum dry densities, and a high optimum moisture content have been observed. All these values are adopted for the evaluation of this material as a structural filling with cement additives. Moreover, this approach could chemically stabilize the material against biodegradation (Stylianou et al., 2018)(Arulrajah et al., 2014).

SCG and polymeric composites

Another field of study, that has been developed in recent years, foresees the SCG as a reinforcing material in polymeric composites. Even though this material presents two main issues due to its lignocellulosic and hydrophilic nature, which promote poor particle dispersion and dimensional dispersion, some researchers have been able to produce biocomposites. Such is the case polypropylene (PP) with 20% by weight of SCG, previously treated with a derivative of palmitic acid

(hydrophobic method) to reduce the absorption of water and improve the particle dispersion (Lascano et al., 2020). Furthermore, SCG was used as a bio-reinforcing agent in a weight percentage of 10% for biodegradable poly(butylene adipate-co-terephthalate) (PBAT), to produce new material for food packaging (Stylianou et al., 2018).

SCG for biodiesel production

Biodiesel is a renewable and biodegradable fuel, used instead of fossil fuel or added to it in internal combustion engines. The main objectives in the use of this type of diesel are the reduction of environmental pollution, with a consequent increase in renewability, and the reduction of dependence on fossil fuels. In recent decades, its demand from European countries has grown to achieve national and international goals.

The most important process for producing biodiesel is transesterification, a reaction between triglycerides and low molecular weight alcohol (ethanol or methanol) in the presence of a basic catalyst (NaOH or KOH) to obtain esters and glycerol. SCG has a lipid content of 10-20 %, which can be exploited for the production of biodiesel. Bioethanol is added to the lipid fraction and, through the transesterification reaction, the final fuel is obtained. It is estimated that 1 billion litres of biodiesel per year can be produced from SCG. For this reason, there are currently several studies to identify the best method for lipid extraction from the SCG, and on how to manage the residual biomass after the extraction (Nídia S. Caetano et al., 2014)(Nídia S. Caetano et al., 2012).

Different studies have shown that crude lipids extracted from SCG can be transformed into fatty acid methyl ester (FAME) and fatty acid ethyl ester (FAEE) by a non-catalytic transesterification process. (Al-Hamamre et al., 2012). In particular, some researchers (N. S. Caetano et al., 2017) have explored the extraction of oil from SCG using hexane. Despite, the relatively low oil extraction (6.5%) and the high acidity value (44.8 mg of KOH g^{-1} oil), the final yield value was 96.7%, with 87.6% of esters (45 °C). Using 92% of ethanol, could increase both the yield and the ester content with percentages of 97.2 and 92.1% respectively.

Other important studies are related to the transesterification in situ (TE in situ), a process that doesn't involve the use of hexane, for the generation of biodiesel in an on-site SCG source (Tuntiwiwattanapun et al., 2017). The total evaluation of this process showed greater environmental impacts than the conventional process, which required 43% less energy. It has, therefore, concluded that the use of this process is convenient only on transport distances greater than 180 km with 7 $\frac{km}{L}$ fuel consumption rate.

In addition, it was discovered that it's possible to obtain hydrocarbon (diesel) generation from SCG (Döhlert et al., 2016). The catalytic hydrodeoxygenation of coffee oil is achieved by applying polymethylhydrosiloxane (PMHS), as a low-cost reducing agent under non-extreme conditions. However, PMHS is considered as a by-product, because only 1.7% is required for the reduction reaction. It's further transformed into methyltrifluorosilane and difluoromethylsilane to be used as building blocks for the production of silicones.

Source of energy

If properly treated, the SCG can be used in boilers as a combustible material, thanks to its high calorific value, and involve a direct energy source. According to the International Coffee Organization (ICO), for

energy application of the SCGs, they must be pelletised. For this purpose, the moisture content should be between 11 and 12.5% to avoid the deformation of moulds, while a moisture content between 10 and 10.5% is recommended to ensure safe storage and the elimination of growth of microorganisms during saving at the warehouse temperature (Tun et al., 2020).

In this line, has been examined the possibility of using SCG to produce thermal energy to generate roasted coffee (Allesina et al., 2017). According to the industrial plan, a small Italian roasting company will completely cover its heating needs through the combustion of wood-coffee pellets in 4 years and the CO_2 emissions generated will be substantially reduced (Stylianou et al., 2018). However, the direct use of SCGs may involve positive but also negative effects. For example, if not treated, combustion gases may lead to the production of atmospheric pollutants, such as carbon monoxide (CO) and volatile organic compounds (VOCs), which are harmful to human health.

3. Materials and methods

In this chapter, the materials and experimental procedures for the kinetic analysis are overviewed.

3.1. Materials

The spent coffee grounds (SCGs) analysed are the residue obtained by the preparation of the coffee drink, by filtering the coffee powder with hot water at ~80 °C. The spent coffee grounds were left for water draining at ~20 °C overnight and subsequently dried in the Heraeus LUT6050 convection oven at 105 °C for 2 h to remove moisture. **Figure 3.1** shows the macroscopic appearance of the SCGs.

Figure 3.1: Macroscopic appearance of SCGs

The **Table 3.1** presents data for proximate analysis, ultimate analysis, and calorific value, previously determined for this material (Primaz, 2018).

Table 3.1:Proximate analysis, ultimate analysis and calorific value of SCGs (Primaz, 2018).

Proximate analysis	
Moisture (%)	11.37 ± 0.08
Ash yield (%)	2.24 ± 0.58
Volatile matter (%)	93.84 ± 0.58
Fixed Carbon (%)*	3.92 ± 1.06
Ultimate analysis	
N (%)	2.79 ± 0.08
C (%)	49.18 ± 0.05
H (%)	6.52 ± 0.29
O (%)*	41.51 ± 0.42

H/C	1.59 ± 0.07
O/C	0.63 ± 0.01
Calorific Value	
HHV (MJ/kg)	20.46
LHV (MJ/kg)	19.25

**calculated by the difference*

The ultimate analysis reveals a high content of carbon and oxygen in the biomass, which is indicative of its lignocellulosic structure. The high percentage of carbon also implies high values of calorific values. This means that for energy production in thermo-chemical conversion processes, this type of biomass can be considered sustainable.

Concerning the nitrogen, it should be noticed its low content. This result suggests the improbable production of NO_x compounds during combustion. Therefore, coupling this value with the low percentage of ash yield, obtained in the proximate analysis, can be promoted the use of this material in the production of bioenergy.

3.2. Thermogravimetric analysis (TGA)

The definition given by the TURI for thermogravimetric analysis is “a technique in which the mass of the sample is measured as a function of temperature, while the sample is subjected to a controlled temperature program”(*Confederación Internacional Para El Análisis Térmico I.C.T.A Internacional Commitee Thermal Analysis*, n.d.). The mass loss is correlated to chemical processes or the removal of volatile compounds. The TGA analysis may be performed in two different modes, dynamic and static. In the first case, a heating program at a constant rate is set, while in the second one, the heating program is a function of the time at a fixed temperature. Constant heating rates are typically in the range from 5 to 20 °C·min^{-1}. For commercial TGAs, the working temperature range is between 20 °C (ambient temperature) and 1000 °C. Moreover, the atmosphere of the analysis may be simulated by selecting the particular gas that flows through the balance, and can be inert, oxidizing, or reducing. The first is composed of nitrogen, argon, or helium; the second of air or oxygen, and, finally, the third of forming gas (8–10% hydrogen in nitrogen). When carried out in an inert gas atmosphere, TGA is useful in ranking the relative thermal stability of polymers and to observe the formation of char residues.When it is carried out under oxygen or air atmospheres, it's also possibleto analyse the emission of gases and residuesthat remain as ashes of carbon, metallic oxides or of salts that cannot be oxidized. This case is called thermo-oxidative decomposition.

Data from TGA are shown by a graph, called a thermogram, representing mass as a function of temperature for dynamic case, and mass as a function of time at a given temperature, in the static approach. Generally, the chart corresponds to a sigmoidal curve with one or more stages, depending on the sample composition and the chemistry of components. Typically, between 50 °C and 150 °C, it's possible to detect the loss of volatile components such as water, organic solvents with low molecular weight, or absorbed gases (Menczel & Prime, 2008). After that, in the range of 150-250 °C, occurs the loss of low molecular weight components like additives, crystallization water, plasticizers, or first decomposition products. Between 225 °C and 250 °C, the thermal degradation starts, and depending on the type of the atmosphere present, it could follow different routes. At temperatures above 500

°C, hydrocarbonated compounds are charred because their thermal decomposition does not lead to the formation of volatile fragments. A residue may be found together with non-degradable fillers or inorganic additives.

The derivative of the thermogravimetric curve is defined as DTG. This curve is useful to distinguish the overlapping of mass losspeaks, to identify the shape and maximum of mass loss processes, and to detect minor mass loss steps. The DTG maximum peak defines the maximum rate of mass loss. Each peak in the DTG represents a separate peak. The DTG curve is a sensitive measurement and gives information on the relative rates of volatilization and polymer decomposition. This technique allows the study of the thermal decomposition of polymers, the decomposition rate, the reaction order, and the activation energy, but also the determination of additives and fillers present in complex formulations.

In this work, the thermogravimetric analysis was conducted to characterise the thermo-oxidative decomposition process of the biomass and the pyrolytic behaviour and to obtain the temperature range in which the main mass losses occur. The analyses were performed on a Mettler Toledo TGA/SDTA 851 module (Columbus OH), shown in **Figure 3.2**. Samples of approximately 7 mg were heated on alumina crucibles with a capacity of 70 µL. The experiments were performed in the temperature range of 25 °C to 800 °C at a heating rate of 2, 5, 10, 15 and 20 °C·min^{-1}, first under an oxidative atmosphere of oxygen and second in an inert atmosphere of argon, at a gas flow rate of 50 mL·min^{-1}. The obtained results were evaluated using the STARe 9.10 software. Three specimens of each sample were analysed and the averages were considered.

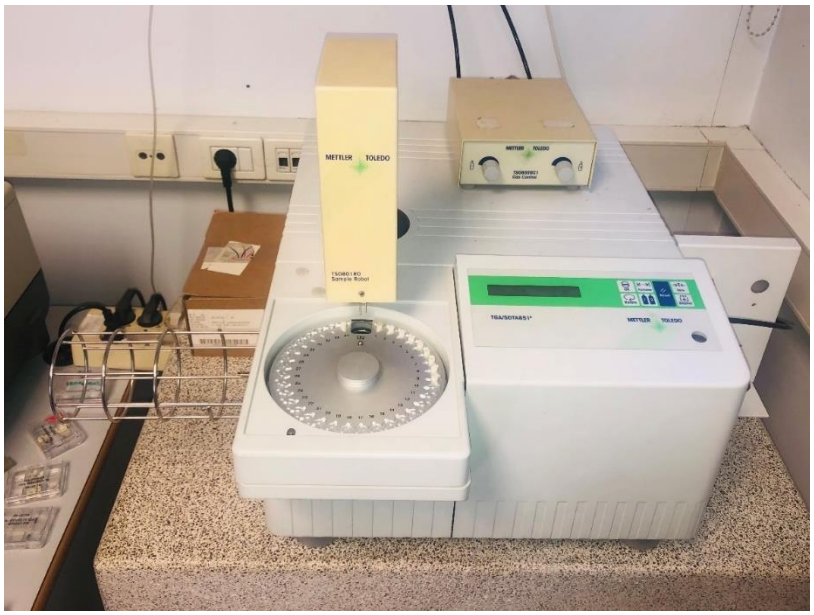

Figure 3.2: Mettler-Toledo TGA 851 series with 70 µL alumina capsules containing ash.

3.2.1. Deconvolution analysis

In thermogravimetry (TG–DTG) experiments, several reaction regions may be found, related to the decomposition of different pseudo-components and subsequent degradation by-products that can be grouped in (*i*) volatilization reactions and (*ii*) char-forming reactions. The deconvolution analysis allows identifying in the DTG graph the peaks corresponding to the different stages and pseudo-components

of the biomass, through the application of a multi-step model and an analytical approach, involving the deconvolution of the individual pseudo-component peaks. The starting hypothesis is to consider that the process occurs simultaneously and therefore the curve obtained is the sum of the theoretical individual curves, which lead to a computed DTG curve and the reactivity of decomposition regions is proportional to the height of the DTG peak (Kok & Özgür, 2013). In this study, this analysis was carried out considering that (*i*) the degradation temperature ranges of water and the three main constituents of biomass (hemicellulose, cellulose, and lignin); (*ii*) the decomposition of each component takes place in a single step; and (*iii*) the thermal decomposition of the sample is the sum of independent reactions.

The model curves are meant to reproduce the experimental DTG curve by the minimization of the differences between their ordinates, through a criterion such as least-squares (Rego et al., 2019). As examples of the most common theoretical functions that can be used for deconvolution, it is possible to mention the Gaussian function, the Lorentz function, the Asymmetric Double Sigmoidal function, the Laplace function, or the Pearson VII function. To perform the analysis, it is important to consider the assumption of the so-called pseudo-component model, which is used to simplify the quantification of components that, in reality, are strongly interconnected within the anatomical structure of lignocellulosic biomass. It does not produce significant deviations from the reality of biomass thermal decomposition (Rego et al., 2019).

The ranges of the temperature degradation are influenced by the atmosphere present and, generally, there is a difference between oxidative and inert. Theoretically, low heating rates allow better separation of degrading components in less time. Conversely, high heating rates get worse the separation of the lignocellulosic fractions, making the identification difficult. However, to obtain validation of the method, it is necessary to simultaneously develop the analysis at very different rates.

In this work, the deconvolution of the DTG curves was carried out by using the multipeak Lorentz fitting method. The OriginPro 9 software was used to carry out the deconvolution computation of the DTG curves. In particular, the overlapping peaks were separated into five sub-peaks, corresponding to water, hemicellulose, cellulose, lignin, and char. The fitting was performed therefore by optimization of three parameters: x_c, center; A, amplitude; and ω, width at half of the maximum height, according to Equation **(3.1)**:

$$y = y_0 + \frac{2A}{\pi} \cdot \frac{\omega}{4(x - xc)^2 + \omega^2} \qquad \textbf{(3.1)}$$

where x is the independent variable an y_0 is the initial value of the Lorentz function at x_0.

3.3. Kinetic analysis of the thermal and thermo-oxidative decomposition of biomass

This section, the description of the kinetic analysis conducted on the material is described. This analysis is characterized by the definition of kinetic triplet, involving activation energy (Ea), pre-exponential factor (A), and kinetic function ($f(\alpha)$).

To determine the chemical changes occurring in the system, the thermal decomposition rate equation has two different contributions, the reactant concentration and the reaction rate (k), that depends on the absolute temperature.

$$Thermal\ decomposition\ rate = f(reactant\ concentration) * k(temperature)$$

The reaction rate (*k*) is described by the Arrhenius equation, while the reactant concentration at every moment in the thermal decomposition process is represented in terms of mass loss at every time (ω). Therefore, ω is the function dependent on the concentration, through which it's possible to define the kinetic equation.

A complementary feasible strategy to solve the kinetic equation is defining the reactant concentration through the conversion degree (α), equal to the ratio between the sample mass lost at a time t and the sample mass lost at an infinite time or total mass loss.

The Arrhenius equation, the kinetic equation, the decomposition degree, and the rate equation are all reported in **Table 3.2**, where *R* is the universal gas constant; *T* is the absolute temperature; E_a is the activation energy; *A* is the pre-exponential factor, assumed independent of temperature; ω is the actual (at time *t*) mass of the sample; ω_0 is the initial mass of the sample; ω_∞ is final mass of the sample. For the final determination of the rate equation is important to underline that $f(\alpha)$ depends on the mechanism of the degradation reaction.

Table 3.2: Equations applied to determine the final rate equation (Greus et al., 2008).

Arrhenius Equation	
$$k(T) = A * \exp\left(-\frac{Ea}{RT}\right)$$	**(3.2)**
Kinetic Equation	
$$\frac{d\omega}{dt} = -\omega * A * \exp\left(\frac{\mathrm{E}}{\mathrm{RT}}\right)$$	**(3.3)**
Decomposition degree	
$$a = \frac{\omega 0 - \omega}{\omega 0 - \omega\infty}$$	**(3.4)**
Rate Equation	
$$\frac{da}{dt} = f(a) * k(T) = f(a) * A * \exp\left(-\frac{E}{RT}\right)$$	**(3.5)**

Table 3.3 provides some examples of the most commonly used differential functions $f(a)$ and integral *g(a)* (Khawam & Flanagan, 2006) to develop a thermal and thermo-oxidative decomposition model of a full-scale system. In these equations, mass and heat transfer limitations are absent, since they are the result of a simplified reaction pathway, in which only the behaviour of the reaction in terms of intrinsic kinetics is considered, and not the whole complex network of reactions that characterizes each reaction phase.**Table 3.3:** Algebraic expressions for the differential f(α) and integral g(α) functions for used mechanisms of solid-state processes.

Symbol	f(α)	g(α)	Solid-state processes
Sigmoidal curves			
A_2	$2(1-\alpha)[-\ln(1-\alpha)]^{-1}$	$[-\ln(1-\alpha)]^{\frac{1}{2}}$	Nucleation and growth (Avrami equation 1)
A_3	$3(1-\alpha)[-\ln(1-\alpha)]^{-1}$	$[-\ln(1-\alpha)]^{\frac{1}{3}}$	Nucleation and growth (Avrami equation 2)
A_4	$4(1-\alpha)[-\ln(1-\alpha)]^{-1}$	$[-\ln(1-\alpha)]^{\frac{1}{4}}$	Nucleation and growth (Avrami equation 3)
Deceleration curves			
R_1	1	α	Phase boundary controlled reaction (one-dimensional movement)
R_2	$2(1-\alpha)^{\frac{1}{2}}$	$\left[1-\ln(1-\alpha)^{\frac{1}{2}}\right]$	Phase boundary controlled reaction (contracting area
R_3	$3(1-\alpha)^{\frac{2}{3}}$	$\left[1-ln(1-\alpha)^{\frac{1}{3}}\right]$	Phase boundary controlled reaction (contracting volume)
D_1	$\frac{1}{(2a)}$	α^2	One-dimensional diffusion
D_2	$\frac{-1}{\ln(1-a)}$	$(1-\alpha)\ln(1-\alpha)+\alpha$	Two-dimensional diffusion
D_3	$\frac{3(1-a)^{\frac{2}{3}}}{2[1-(1-a)^{\frac{1}{3}}]}$	$\left[1-(1-\alpha)^{\frac{1}{3}}\right]^2$	Three-dimensional diffusion
D_4	$\frac{3}{2}[(1-a)^{\frac{1}{3}}-1]$	$\left[1-\frac{2}{3}a\right]-(1-a)^{\frac{2}{3}}$	Three-dimensional diffusion
F_1	$1-\alpha$	$-\ln(1-\alpha)$	Random nucleation with one nucleus on the individual particle
F_2	$(1-\alpha)^2$	$\frac{1}{(1-\alpha)}$	Random nucleation with two nuclei on the individual particle
F_3	$\frac{1}{2}(1-\alpha)^3$	$\frac{1}{(1-\alpha)^2}$	Random nucleation with three nuclei on the individual particle

3.3.1. Calculation of the activation energy

The activation energy (E_a) can be calculated adopting different models based on the analysis at multiple heating rates, assuming the given kinetic function and mathematical treatment of the general kinetic law, in terms of differential or integral approach.

In this study, two different approaches were considered, involving differential and integral methods. Both were based on linear methods for the determination of the activation energy based on multiple thermogravimetric experiments at different heating rates and atseveral conversion degrees, where the kinetic parameters can change during decomposition. This variation is demonstrated through iso-conversional methods, that use data from different multi-linear non-isothermal experiments and do not take model assumptions for the analysis. The integral methods are characterized by an estimated integration of the integral function of conversion $g(\alpha)$ while the differential considers the differential function *f(α)*. All the methods proposed are reported in **Table 3.4**. (Ozawa, 1965)(Friedman, 2007)(Vol et al., 1988).

Table 3.4: Equations used for the calculation of the activation energy.

Differential methods	
Flynn- Wall - Ozawa (FWO)	
$log\beta = \log(\frac{EA}{R * g(a)}) - 2.315 - \frac{0.457\ E}{RT}$	**(3.6)**
Kissinger-Akahira-Sunose (KAS)	
$[ln(\frac{\beta}{T^2})]y\ =\ ln(\frac{Aa * R}{Ea_a * g(a)}) - \frac{Ea_a}{R} * [\frac{1}{Ta}]x$	**(3.7)**
Integral method	
Friedman	
$[ln(\frac{da}{dt})a]y\ =\ ln\big(Aa * f(a)\big) - \frac{Ea_a}{R}\ * [\frac{1}{Ta}]x$	**(3.8)**

3.3.2. Analysis of kinetic function

For the calculation of the Kinetic function, the use of Master-Plots (MP) was considered. This method is characterized by the use of theoretical curves (M-P_t), which is independent of the kinetic parameters of the process but shown a dependence on the kinetic model. To obtain a good selection of the most appropriate kinetic model of the process, it is possible to transform the TGA data into experimental curves (M-P_e) and make a comparison with the M-P_t curves. There are three main types of reference theoretical curves, based on the differential form (M-P_f), on the integral form (M-P_g), or the combination of both differential and integral forms (M-P_{fg}) of the generalized kinetic equation. As described by Criado, these curves are usually reduced considering the factor α = 0.5 to obtain a better visualization (Criado et al., 1989).

Then, the kinetic analysis can be carried out with a single step kinetic equation **(3.9)** considering the activation energy found using the iso-conventional methods previously described.

$$\frac{da}{dt} \equiv \beta * \frac{da}{dt} = A * f(\alpha) * k(T) = A * f(\alpha) * e^{\frac{-Ea}{RT}} \quad \textbf{(3.9)}$$

Developing the integral of the equation **(3.10)**, the inverse integral kinetic function $g(\alpha)$ is obtained:

$$g(\alpha) = \int_0^a \frac{da}{f(a)} = \frac{A * Ea}{\beta * R} * \int_0^\infty \frac{e-x}{x^2} = \frac{A * Ea}{RT} \cdot p(x) \quad \textbf{(3.10)}$$

where $x = \frac{E}{RT}$; and $p(x) = \frac{e-x}{x^2} * \sum_n \frac{n*(1-n)}{x+2*(n+1)}$ is the Senum-Yang approximation.

The Senum-Yang approximation was truncated in the fifth term. This operation leads to a good approximation for the exact temperature integral for x > 10 (Pérez-Maqueda & Criado, 2000).

By plotting the experimental curves (M-P_e) at different α, it is possible to obtain the final curve and develop the graphic comparison with the theoretical master curves. The **Figure 3.3**. shows the Master-Curves present in **Table 3.3**, both in differential and integral form.

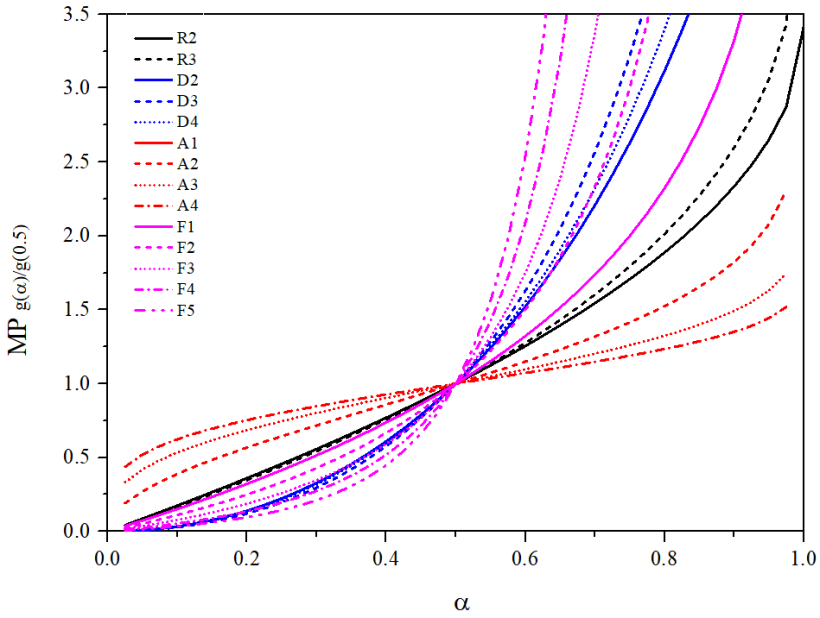

Figure 3.3: Criado master curves for some of the kinetic models shown in **Table 3.3.**

3.3.3. Analysis of pre-exponential factor

The last step is the determination of the pre-exponential factor (A). For this purpose it is important to satisfy the Perez-Maqueda criterion (P-Mc) (Pérez-Maqueda et al., 2002). This includes the independence of the activation parameters E_a and A with respect to the heating rate (β). The criterion considers Ea and A invariable and is coupled with the Coats-Redfern's equation (Coats. A.W., Redfern, 1964):

$$\left[ln\frac{\beta * g(a)}{T^2}\right]_y = ln\frac{AR}{Ea} + \frac{Ea}{R} * \left[\frac{1}{T}\right]_x \quad \textbf{(3.11)}$$

In this work, the Perez-Maqueda criterion was applied, after the calculation of the activation energy from iso-conversional methods and the determination of reaction mechanism, using master plots. At this point, the best *n* order of the kinetic model was established by minimizing the equation **(3.12)**.

The points {x, y}, obtained through the equation **(3.11)** with the best *n*, have to lie on the same straight line to all heating rates. The pre-exponential factor (*A*) results, finally, to be the average of the values A_β from the intercept at *y = 0* of the Coast-Redfern equation.

$$\xi(\mathrm{n},\alpha) = \sum_i^h \left|(-R) * \frac{d}{dt}\left(\frac{\ln(\beta_i * T^{-2} * g(a)}{T^{-1}}\right) - Ea_{iso}\right| \quad \textbf{(3.12)}$$

4. Results and discussion

In this section, the results obtained for the SCG are shown, described, and discussed. Particularly, the thermal and thermo-oxidative decomposition analysed in the inert and oxidative atmospheres were studied. Then, from the DTG graphs, a deconvolution analysis was applied. Considering that the general composition of woody biomass and the common temperature ranges for the degradation of the different constituents of the biomass are known from the literature, hypothetical peaks related to the decomposition of pseudo-components (hemicellulose, cellulose, and lignin) were assessed. Finally, the kinetic analysis for the decomposition was carried out, involving the determination of the activation energy, the kinetic function assessment, and the pre-exponential factor determination.

4.1. Thermo-oxidative decomposition under combustion conditions

4.1.1. Thermo-oxidative stability

The thermo-oxidative stability was assessed for the sample at different heating rates (β) of 2, 5, 10, 15, and 20 °C·min^{-1} to study the behaviour of SCG in an oxidative atmosphere. The mass loss in the different regions, the temperature related to the peaks, the onset/endset temperatures, and the zero-decomposition temperature were evaluated. This last value allows predicting the behaviour of the sample when the heating rate tends to zero, avoiding the influence of the dynamic heating program.

The obtained thermogravimetry (TG) and its first derivative (DTG) curves are shown in **Figure 4.1**. Starting from these curves, the onset and endset degradation temperatures (T_o, T_e), the peak temperature (T_p), and the mass loss percentages for each stage (Δm) were obtained, which values are gathered in **Table 4.1.**

During the heating, it is visible on the TGA chart a progressive decreasing trend, that corroborates the mass loss. The thermogram is divided into different mass loss regions, corresponding to the decomposition of biomass constituents. The initial mass reduction, with a contribution of 6-8% from 25 °C to 140-150 °C, is related to the moisture vaporization. This step is followed by a stage of decomposition connected to the devolatilisation of volatile hydrocarbons present inside the hemicellulose and cellulose. This is characterized by mass loss of 55-57% and takes place between 170-180 °C and 350-360 °C, respectively. The two components are evaluated together because their decomposition occurs overlapping the peaks in the DTG charts. Then, it is possible to find the step related to the decomposition of lignin. It happens between 340-360 °C and 420-460 °C, with a mass loss of 20-25%. The last decomposition of char occurs above 425-460 °C and the mass loss is 13-17%. After it, the degradation continues quite fast until temperatures of 550-650 °C, where almost complete decomposition is reached. A residue (R) at the end of the analysis may be ascribed to the remnant ash. The obtained values, between 0.5 and 2 are in concordance with the ash percentage reported in the proximate analysis of SCGs.

When the heating rate increases, the decomposition temperature range is moved towards higher values. It means that the heating rate affects both the shape of the TGA curve and the location of the maximum DTG peaks. At low values of heating rate, the peaks are enough visible, while increasing the heating rate some peaks merge with others, and it is not possible to clearly distinguish them. This phenomenon can be explained through heat transfer limitations. During the analysis, at a low heating rate, a larger instantaneous thermal energy is provided to the system and a longer time is required for

the purge gas to reach equilibrium with the temperature of the furnace of the sample. While at the same time and in the same temperature region, a higher heating rate has a shorter reaction time, and therefore the temperature needed for the sample to decompose is also higher. This causes the shifting to the higher temperature of the curve obtained with the highest heating rate (Kongkaew et al., 2015).

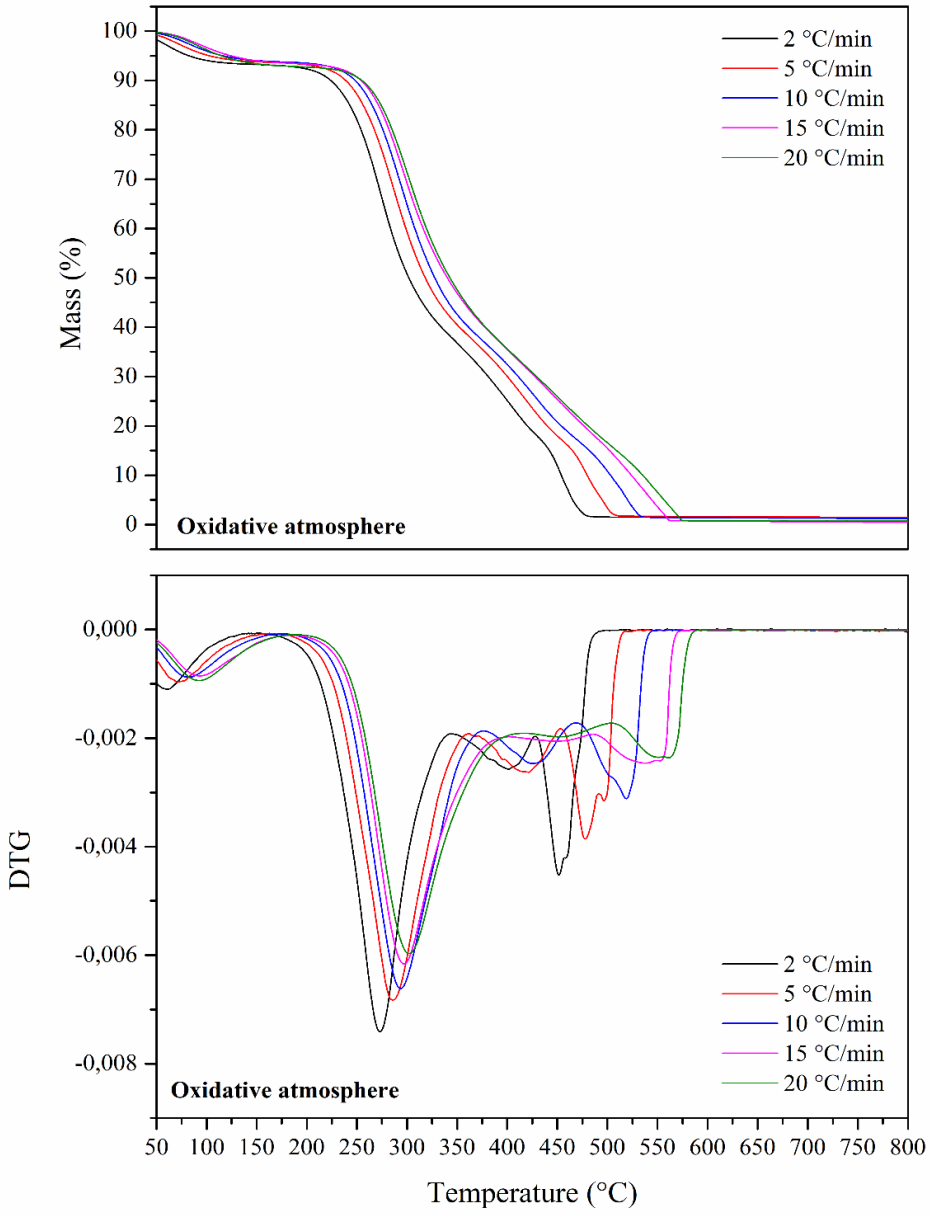

Figure 4.1: Thermogravimetry (TG) and their derivative (DTG) curves of SCG samples under oxidative conditions at β of 2, 5, 10, 15, 20°C·min^{-1}

As expected from the observation of the TG and DTG curves, increasing the heating rate displaced all the characteristic decomposition temperatures (onset, endset, and peaks) towards higher values.

As suggested before, inside the main peak associated with the hemicellulose, it's visible a small shoulder related to the overlap of the peaks of cellulose and hemicellulose. Due to the impossibility to have a clear distinction, one peak temperature T_{p1} and one mass loss Δm_1 are considered at this point. Subsequently, T_{p2} and T_{p3} are associated with the peak temperatures of lignin and char.

For a graphical interpretation of the contribution of the heating rate, the decomposition temperatures T_e, T_o and the peak temperatures T_{p1}, T_{p2} and T_{p3} are plotted in **Figure 4.2**.

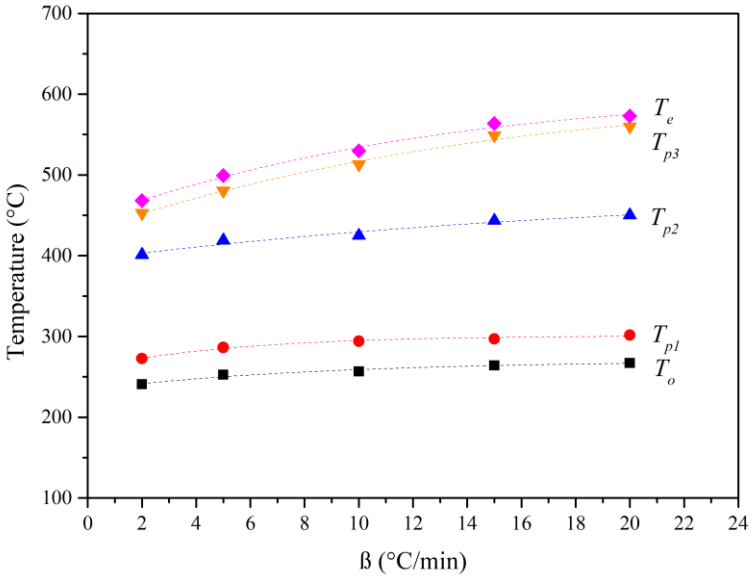

Figure 4.2: Evolution of the characteristic decomposition temperatures T_o, T_e, T_{p1}, T_{p2} and T_{p3} at at β of 2, 5, 10, 15, 20 °C·min^{-1}.

From the representation of characteristic temperatures against the heating rate, the zero-decomposition temperature (ZDT) can be calculated when the heating rate tends to zero. For this purpose, the exponential relationship shown in **Equation 4.1** may be considered, where *a, b* and *k* are the parameters of the fitting. All the obtained TDB values are reported in **Table 4.2**, along with the fitting parameters and the regression coefficients for all the components.

$$ZDT(\beta) = \frac{a}{1 + b * e^{-k*\beta}} \qquad \textbf{(4.1)}$$

Table 4.1: Onset and endset degradation temperatures (T_o, T_e), peak temperature (T_p), and mass loss percentages for the different decomposition of components (Δm) obtained at β of 2, 5, 10, 15, and 20 °C·min^{-1}.

β (°C·min^{-1})	T_o (°C)	T_{po} (°C)	Δm_o (%)	T_{p1} (°C)	Δm_1 (%)	T_{p2} (°C)	Δm_2 (%)	T_{p3} (°C)	Δm_3 (%)	T_e (°C)	R %
2	241	60	6	273	56	401±3	20	453	17	468±1	2.01
5	253	71	6	286	55	419±3	21	480±3	16	499±2	1.37
10	257±2	82	6	294	57	425	22	513±6	14	530±2	1.51
15	264	94	5	297	56	443±6	25	549±10	13	564±1	0.58
20	267	91±1	6	302	55	450±1	23	560±1	14	573±1	1.34

Table 4.2: ZDT ($\beta \rightarrow 0$) values along with the fitting parameters and regression coefficient for T_o, T_e, T_{p1}, T_{p2}, and T_{p3}.

	ZDT (β→0) (°C)	a	b	k	R^2
T_o	235	267±6	0.15	0.13	0.94
T_{p1}	261	301±2	0.15	0.20	0.97
T_{p2}	395	477±44	0.21	0.06	0.93
T_{p3}	431	598±24	0.39	0.09	0.99
T_e	446	601±18	0.35	0.10	0.99

4.1.2. Modelling of the thermo-oxidative decomposition

To fully define the process, identifying the peaks of the pseudo-components of the biomass, with their mass losses and their degradation temperature ranges, the deconvolution analysis was performed, employing the Lorentz function.

Five different peaks, corresponding to five pseudo-components, which are moisture, hemicellulose, cellulose, lignin, and char, were evaluated. The **Figure 4.3** are shown the results of multi-peak fitting obtained for the DTG curves at 2, 5, 10, 15, and 20 °C·min^{-1}. For all of them, the correlation coefficient R^2 between experimental and modeled values, obtained by adding curves of the individual components, has values ranged between 0.95-0.99. It means that the five reactions identified can explain rightly the characteristics of SCG thermo-oxidative decomposition.

According to the data reported in the literature (Ding et al., 2019), the release of the excess moisture occurs between 25 °C and 140-150 °C. The decomposition of the hemicellulose takes place in the range of 175-375 °C, with a peak at 275-300 °C. Cellulose degrades at 250-350 °C, with a peak centred at 320-350 °C, while lignin has a wide degradation temperature range between 350 and 450 °C. It degrades slower for hemicellulose and cellulose. The decomposition of the remaining char occurs in the range of 440-600 °C.

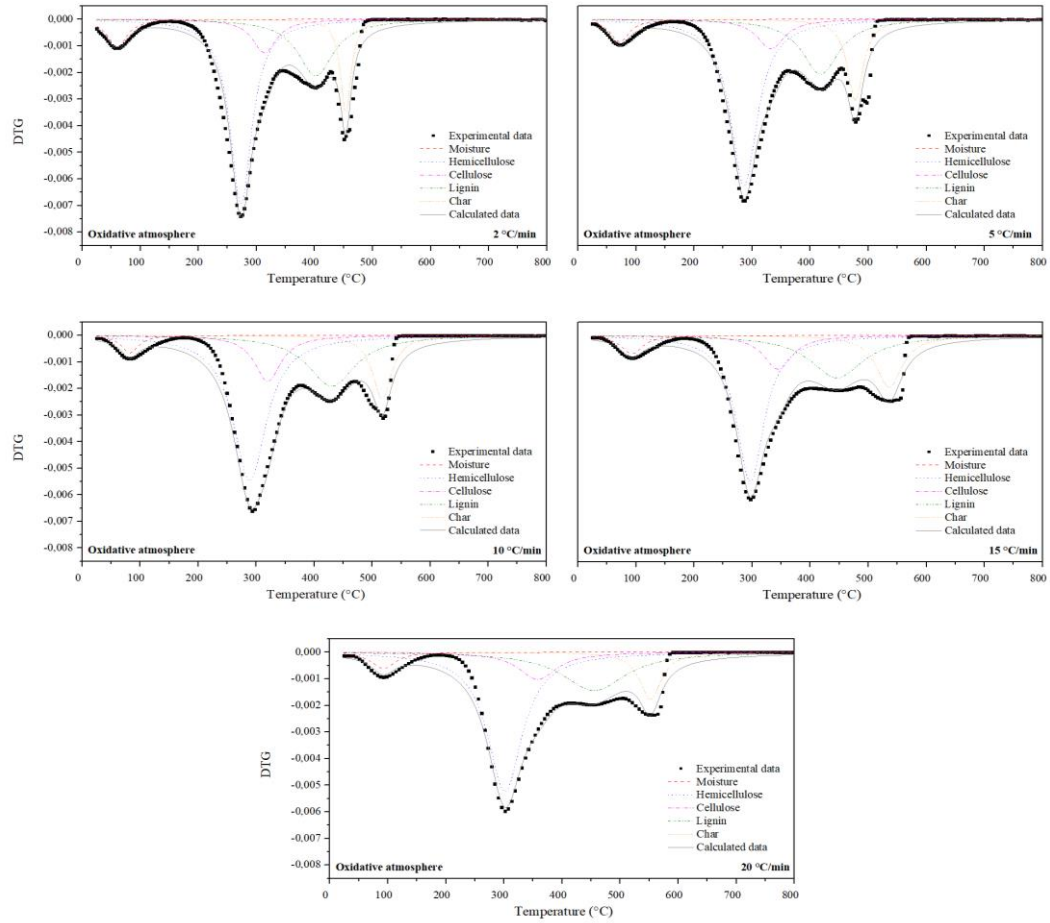

Figure 4.3: The Lorentz function deconvolution results of SCG under oxidative atmosphere at *β* of 2, 5, 10, 15, 20 °C·min^{-1}.

4.1.3. Kinetic analysis of the thermo-oxidative decomposition

In this section, the calculation of the kinetic triplet, obtained by the application of model-free kinetic analyses is given. For this purpose, the results of a set of experimental tests at different heating rates (2, 5, 10, 15, and 20 °C·min^{-1}) were considered.

The activation energy was calculated through model-free methods. Two integral multiple-α methods, described by Kissinger-Akahira-Sunose (KAS) and Flynn-Wall-Ozawa (FWO), and one differential multiple-α model, developed by Friedman, were adopted.

The kinetic function *f(α)* was defined by the use of reduced Master-Plots. To determine the best approximation of reaction mechanisms, both theoretical and experimental reduced curves were plotted and compared.

The pre-exponential factor was calculated using the Coast-Redfern equation, applying the Perez-Maqueda criterion.

Activation Energy

The iso-conversional methods proposed by Friedman, FWO, and KAS, based on multiple thermogravimetric experiments at different heating rates and several conversion degrees, were considered. The conversion degree (α) for the kinetic analysis was selected in the range 0.2-0.8. In this way, considerations of heterogeneous initiation and end-stage reactions were avoided.

It is important to remember that the calculation of the activation energy can be applied to the overall process or a specific peak or aggregation of peaks, defined in temperature ranges. However, in this study, the evaluation of the decomposition reactions of the pseudo-components hemicellulose, cellulose, lignin, and char was carried out. Thanks to the deconvolution analysis reported in the previous section, the peaks related to these pseudo-components were defined and the calculation of the activation energy was directly applied to them.

The activation energy (E_α) at each conversion degree (α), was determined considering the slopes of the tendency lines, drawn for each set of points at different heating rates. **Figure 4.4** shows the linearized plots of hemicellulose, cellulose, and lignin for the three iso-conversional methods. Although activation energy for char could still be evaluated, its linearized plot revealed a low R^2 fitting and therefore it is was omitted.

The fitting lines of the pseudo-components showed a fairly high degree of correlation (R^2) in the range of α from 0.2 to 0.8. While for cellulose R^2 is always between 0.95 and 0.99, it was slightly lower for lignin, with values in the range of 0.92 and 0.98. Regarding hemicellulose, the situation is more complex. In the lower conversion degree (α) range of 0.2-0.3, R^2 is between 0.65 and 0.90, while for α in the range 0.35-0.8, R^2 is between 0.89 and 0.97. Therefore, this observation may be considered for the interpretation of results of the lower conversion degree.

From the slopes of the linear fitting, the apparent activation energies were calculated and are plotted in **Figure 4.5** as a function of the conversion degree.

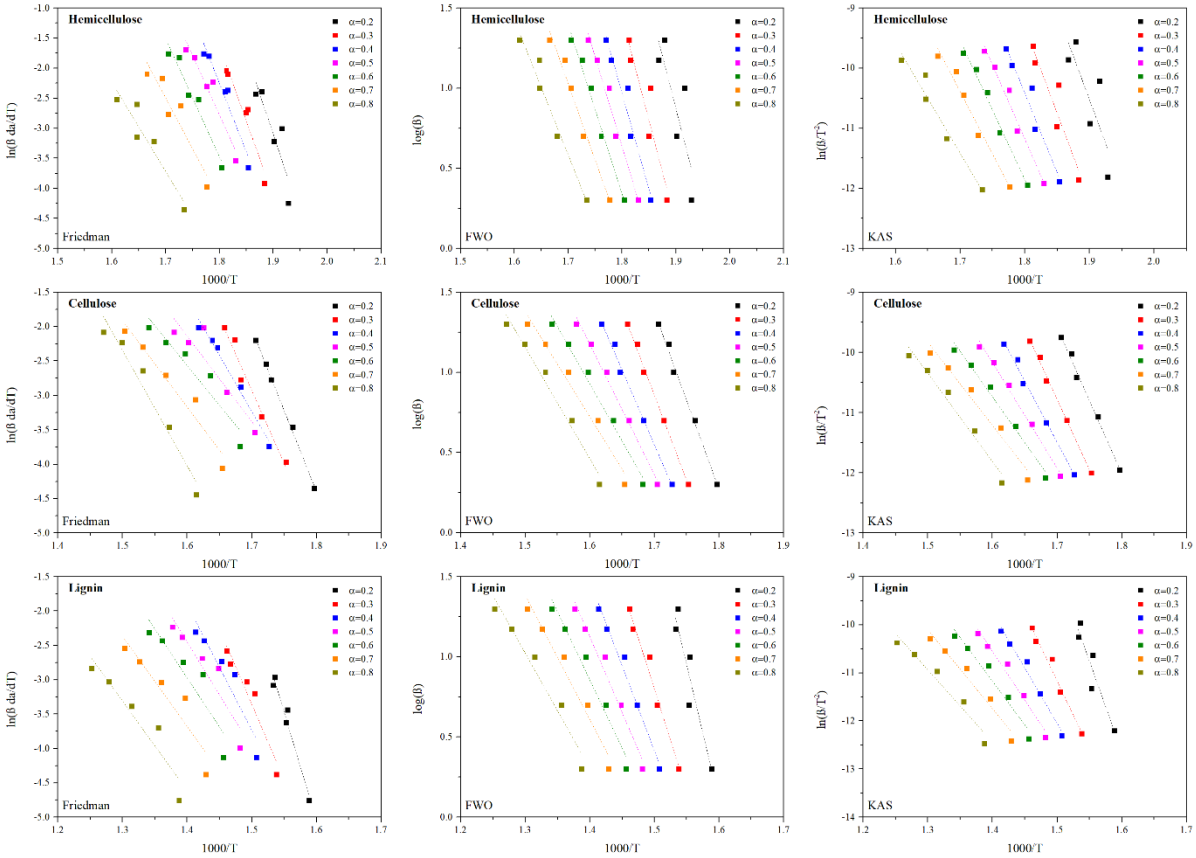

Figure 4.4: Friedman, FWO and KAS fitting plots of hemicellulose, cellulose and lignin for different α.

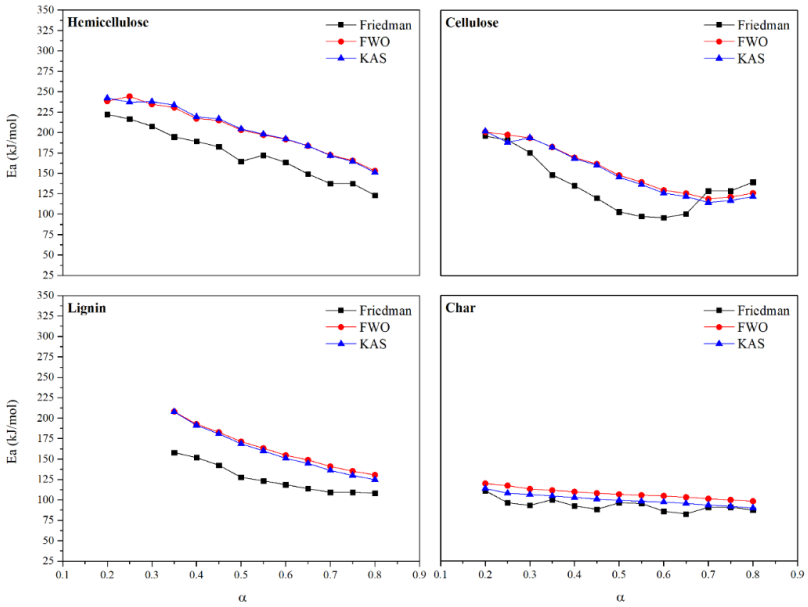

Figure 4.5: Evolution of apparent activation energy in the range of α from 0.2 to 0.8 calculated with different iso-conversional methods for the hemicellulose, cellulose, lignin and char.

The calculated activation energy E_α as a function of α shows a non-constant behaviour. A decreasing tendency was obtained with the advance of the conversation degree. This phenomenon can be justified by the different chemical reactions that occur during the decomposition of a given pseudo-component, which vary when increasing α.

The three iso-conversional methods adopted for the calculation of E_α are dependent on the temperature ranges for the decomposition of the different pseudo-components, which are not constant with β. Indeed, observing **Figure 4.4,** it's possible to see that the degradation temperature ranges become narrower when decreasing the value of β. It must be remarked that these temperature ranges are obtained by the previous deconvolution analysis, where the peaks related to single pseudo-components are defined. Therefore, depending on the temperature ranges selected, the slope of the tendency lines and therefore the activation energy may be slightly different. Considering that each of these tendency lines corresponds to a value of α, the slope decreases from α=0.2 to α=0.8, decreasing the value of E_α. **Table 4.3** collects the average values for the activation energy calculated in the range of conversion degree (α) from 0.2 to 0.8.

Table 4.3: Average values for the activation energy (E_α) obtained with the different iso-conversional methods for hemicellulose, cellulose, lignin and char.

Hemicellulose			**Cellulose**		
$E_{aFriedman}$	E_{aFWO}	E_{aKAS}	$E_{aFriedman}$	E_{aFWO}	E_{aKAS}
(kJ·mol^{-1})	(kJ·mol^{-1})	(kJ·mol^{-1})	(kJ·mol^{-1})	(kJ·mol^{-1})	(kJ·mol^{-1})
174	204	204	135	155	152
Lignin			**Char**		
$E_{aFriedman}$	E_{aFWO}	E_{aKAS}	$E_{aFriedman}$	E_{aFWO}	E_{aKAS}
(kJ·mol^{-1})	(kJ·mol^{-1})	(kJ·mol^{-1})	(kJ·mol^{-1})	(kJ·mol^{-1})	(kJ·mol^{-1})
148	187	184	93	108	100

Regarding the calculation methods,some differences were found in the values of E_α reported in **Table 4.3** which is connected to the different nature of the methods. The Friedman method is differential, while the FWO and KAS are integral. Therefore, after the required numerical differentiation, the results obtained are slightly higher (Moliner, Bosio, et al., 2016).

The average values of apparent activation energy for the different components obtained in this work mostly coincide with those reported in the literature. However, some differences arise, considering the same spectrum of α, which will be discussed below.

The achieved results for the hemicellulose are slightly above the usual average range, but still in the same order of magnitude. With respect to the type of the biomass considered, SCGs, the usual range varies from 105 kJ·mol^{-1} to 155 kJ·mol^{-1} (López-González et al., 2013) (Moliner, Aguilar, et al., 2016). The values calculated for hemicellulose in this work corresponds to 173. kJ·mol^{-1} with the Friedman method, to 203 kJ·mol^{-1} with the FWO method, and 204 kJ·mol^{-1} with the KAS method, as found in **Table 4.3.**

The values of E_a reported in the literature for the cellulose are included in the range 145-195 kJ·mol^{-1}, which comply with the results presented in this work (López-González et al., 2013) (Moliner, Aguilar, et al., 2016).

The E_a values of lignin obtained are in the range from 147 to 187 kJ·mol^{-1}, as reported in **Table 4.3**. Although significant differences may be found in the reported literature range of activation energy may be 55 to 95 kJ·mol^{-1}(Amutio et al., 2012)(López-González et al., 2013) (Moliner, Aguilar, et al., 2016). These differences will be due to differences in the type of biomass and the deconvolution analysis. The decomposition peak of the lignin may be included other reactions, which could affect the calculation of the activation energy of this pseudo-component.

Using the calculated values of the activation energy, the kinetic function and the pre-exponential factor for the thermo-oxidative decomposition will be calculated in the next sections.

Calculation of kinetic function and pre-exponential factor

The most appropriate kinetic mechanism was graphically evaluated for each component of the SCG's, using reduced Master Plots. **Figure 4.6** illustrates the experimental curves at a heating rate of 10 °C·min^{-1} with the theoretical *g(α)* curves, for the typical decomposition mechanisms of biomass reported in **Table 3.3**.

It was observed that all the reaction mechanisms were comparable to the curve of F_n type, with *n* equal to 2, 3, and 4, to D_3 type, or A_2 type. The F mechanisms describe solid-state processes in which random nucleation with one, two, or three nuclei on the individual particle occur, while the D mechanism shows a solid-state process in which three-dimensional diffusion takes place and the A represents a nucleation and growth mechanism.

A mechanism between F_4 and F_5 types was selected for the hemicellulose. For the cellulose, it was difficult to visually determine a single mechanism because the experimental curve falls between F_2 and D_3 models. Finally, according to the reviewed literature for the oxidative decomposition of cellulose, the D_3 type was selected (C. M. Santos et al., 2020). The decomposition of lignin occurred following a model between the F_3 and F_4 type and, finally, the A_2 mechanism was selected for the char. All the mechanisms considered comply with results reported in the literature, in which the decomposition mechanisms of lignocellulosic material components under oxidative conditions are identified as F_n , D_3 or A_2 types, depending on the nature of the biomass (Moliner, Aguilar, et al., 2016) (C. M. Santos et al., 2020).

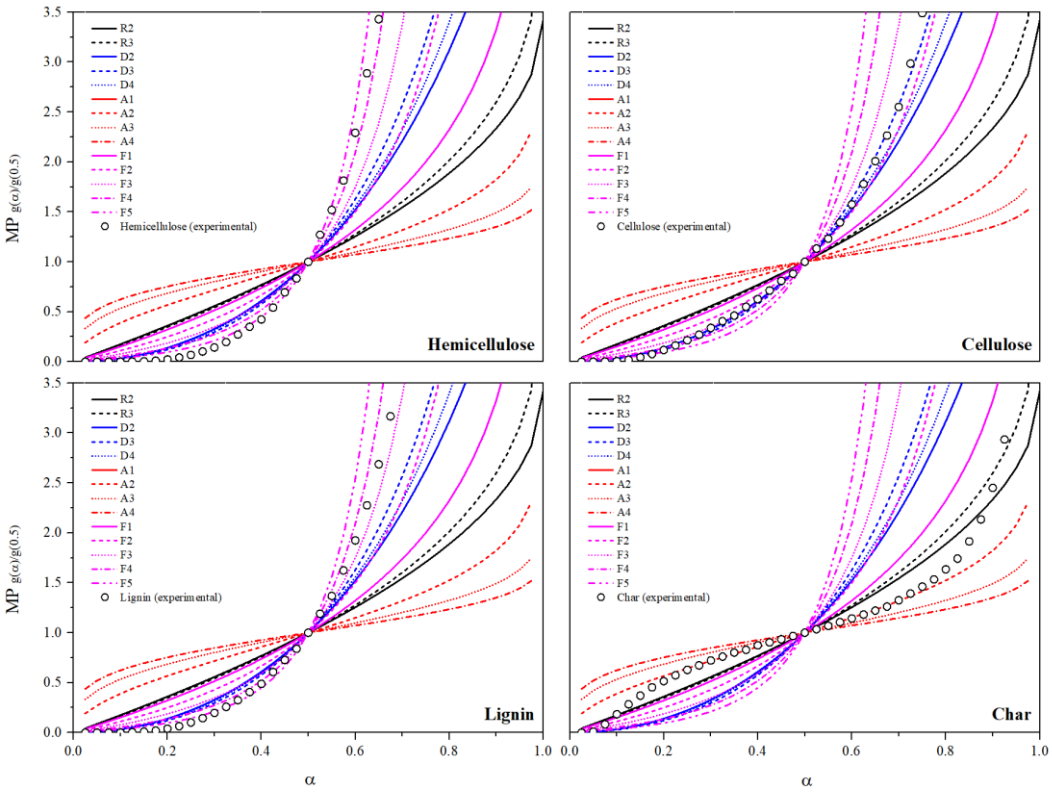

Figure 4.6*:* Normalised Master Plots in comparison to the decomposition process of hemicellulose, cellulose, lignin, and char at a heating rate of 10 °C·min^{-1}.

After the graphic evaluation of the most appropriate theoretical mechanism, the pre-exponential factor *A* was calculated, through the application of the Coast-Redfern equation (**equation 3.11**), and the optimal analytical *n* was estimated for each mechanism. The value of *n* is obtained considering the average value of activation energies for the three iso-conversional methods and applying a regression method.

Then, ln(A) was calculated from the intercept with the axis of the line of the plots $ln(\frac{\beta\, g(\alpha)}{T^2})$ vs $\frac{1000}{T}$, for each heating rate. According to the Perez-Maqueda criterion, the points have to lie on the same straight line, if an adequate $g(\alpha)$ was selected. **Figure 4.7** shows these behaviours for hemicellulose, cellulose, lignin, and char. Moreover, the straight lines in the Perez-Maqueda criterion charts confirm the good fitting of selected mechanisms (F_n, A_2, and D_3).

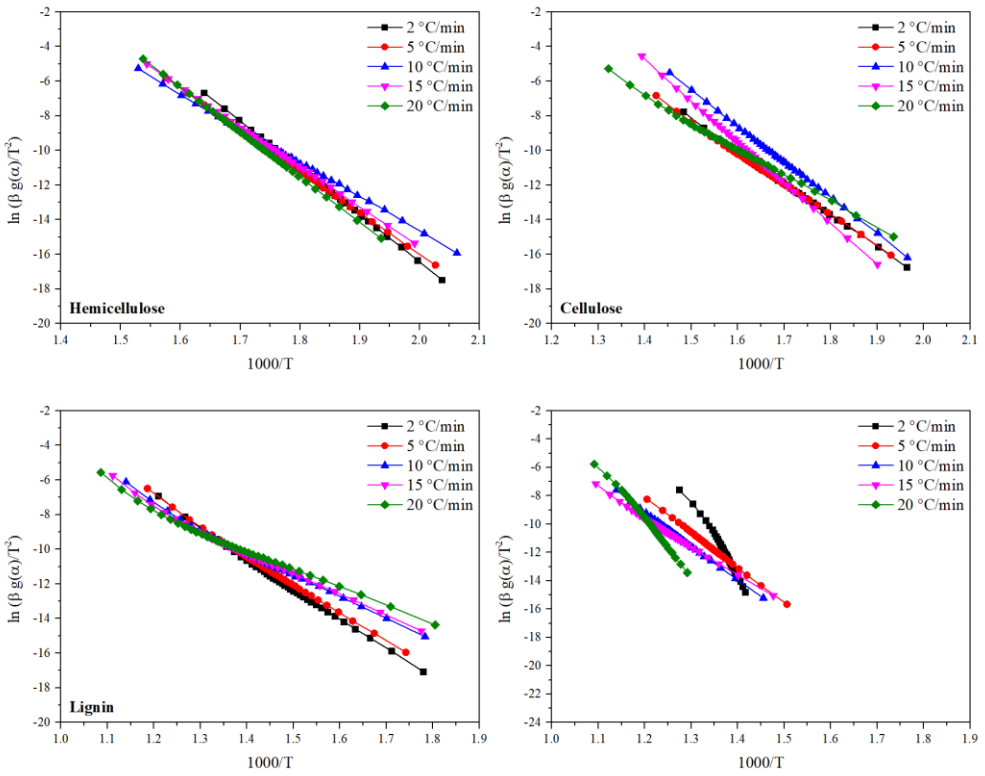

Figure 4.7: Application of the Perez-Maqueda *et al.* criterion for the simplified kinetic triplet of hemicellulose, cellulose, lignin, and char at a heating rate equal to 2, 5, 10, 20, 30 °C·min^{-1}.

For all the components represented in **Figure 4.7,** it is possible to observe a good linearization and accomplishment of the Perez-Maqueda *et al.* criterion. A small deviation is shown in the char, especially at low and high heating rates, justified by the imprecise deconvolution at small and great conversion. Moreover, the decomposition of char involves the most heterogeneous process, given the occurrence of decomposition reactions of all the previously decomposed pseudo-components.

In **Table 4.4** are reported the values for the pre-exponential factor, calculated as an average between the A_β at the different heating rates, for the most appropriate mechanism of the reaction and the calculated analytical order *n* of hemicellulose, cellulose, lignin, and char, under oxidative atmosphere. Furtherly, *e (%)* represents the average of absolute deviations from the mean in each set of ln (A_β).

Table 4.4: Frequency factor *A*, reaction mechanism, and reaction analytical order calculated applying Perez-Maqueda criterion for hemicellulose, cellulose, lignin, and char under oxidative atmosphere.

	Ln(A)	e(%)	n-MP	n
Hemicellulose	41.9	3	F5-F4	3.7
Cellulose	28.3	1.5	D3	-
Lignin	28.6	0.4	F3-F4	3.6
Char	13.5	0.6	A2	-

The obtained results for the pre-exponential factor *A* are in the same magnitude as those reported for lignocellulosic biomass (Moliner, Bosio, et al., 2016). Only the corresponding to lignin shows slightly greater values for the pre-exponential factors due to *A* is strictly related to the activation energy.. The

values of optimal analytical *n* calculated with the regression method confirm the reaction mechanisms selected in the graphical Master Plots.

4.2. Thermal decomposition under pyrolytic conditions

4.2.1. Thermal stability

The thermal stability was assessed for the sample at different heating rates (*β)* of 2, 5, 10, 15, and 20 °C·min^{-1}, to study the behaviour of SCG under an inert atmosphere.

The obtained thermogravimetry (TG) and its first derivative (DTG) curves are shown in **Figure 4.8**. Starting from these curves, the onset and endset degradation temperatures (T_o, T_e), the peak temperature (T_p), and the mass loss percentages for each stage (Δm) were obtained, which values are reported in **Table 4.5**.

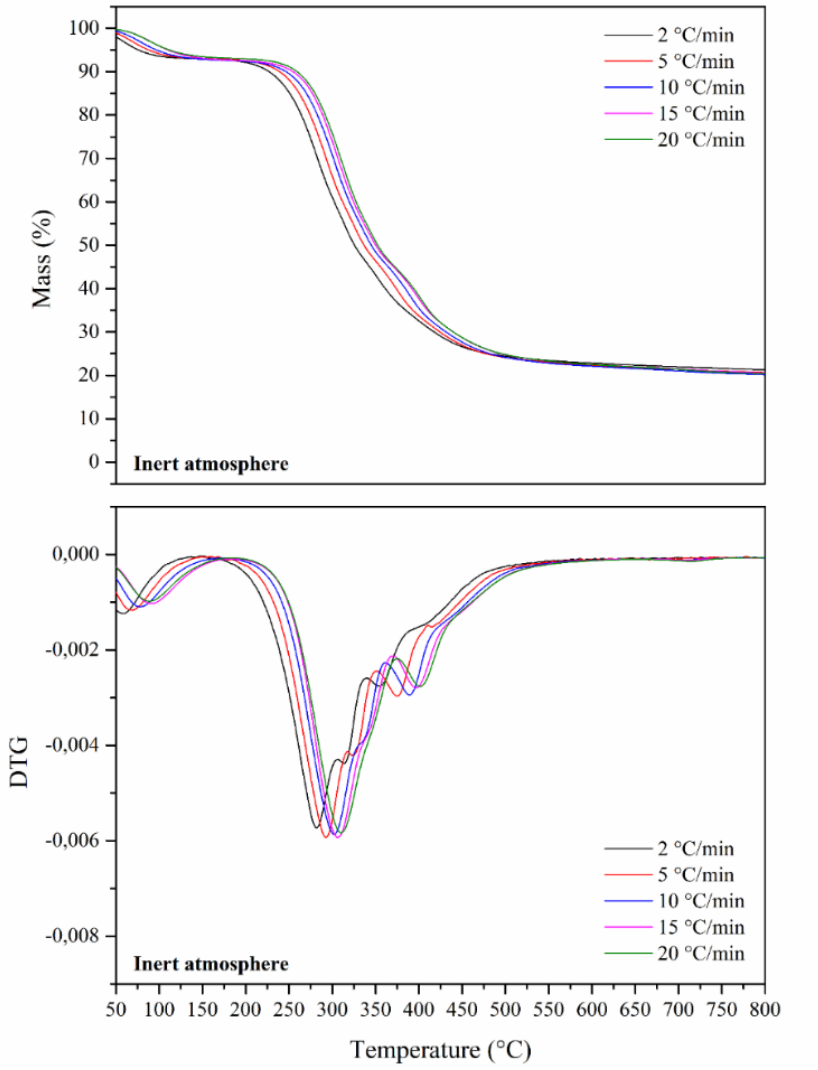

Figure 4.8: Thermogravimetry (TG) and its derivative (DTG) curves of SCG samples under inert conditions at β of 2, 5, 10, 15, 20°C·min^{-1}.

During the heating, TGA thermograms made visible a progressive decreasing trend, that corroborates the mass loss as a function of temperature. The initial mass reduction, with a contribution of 7-8%

from 25 °C to 140-160 °C, is related to the moisture vaporization. This step is followed by the hemicellulose decomposition, which takes place in the range of 160-180 °C to 300-325 °C, with a mass loss of 34-35%. The cellulose decomposition occurs between 300-325 °C and 330-370 °C, with a mass loss ranged between 10 and 12%. Finally, the lignin decomposition appears between 330-375 °C and 410-430 °C, with a mass loss of 10-15%. The last decomposition related to the char is above 430-530 °C. After it, the degradation continues quite fast until temperatures of 530-650 °C, where a residue (*R*) at the end of the analysis may be ascribed to the remnant biochar, with a percentage between 19 and 23%.

Biochar is a carbon-rich, porous solid produced in the process of partial thermochemical decomposition of biomass and represents about 25% by mass, of the original biomass. This solid is the product of elimination of volatile compounds present in the matter that consists of gases, oils and tar. Moreover, some compounds that are not completely degraded may be present, such as carboxylates or salts of carboxylic acids and the possible presence of silicates from the ash (Primaz, 2018).

The microscopic surface structure of the biochar usually shows a material with a carbon matrix relatively structured, large specific surface area, micro, meso and macroporous structure, active functional groups and high pH . These features gives this material a great potential for filtering and adsorbing organic and inorganic pollutants from industrial wastewater and sewage, especially after being physically or chemically activated, and can play an important in the control of contaminants in the environment.

Biochar can also be used as a soil conditioner, which can increase soil fertility and quality, also increasing pH and microbial activity, increasing moisture retention capacity and improving cation exchange capacity, aiding soil maintenance of nutrients. Other advantages associated with the use of biochar as a soil conditioner are the ability to sequester carbon from the atmosphere and transfer it to the soil, offering potential environmental benefits, reducing the need for fertilizers and preventing nutrient loss and erosion.

Furthmore, biochar is also used in the production of briquettes, as it is rich in carbon and has a high calorific value, making the briquette an excellent substitute for charcoal and can be marketed as a household fuel for fireplaces, stoves and also for powering industrial boilers.

The mineral, physical, chemical and mechanical properties depends on the type of raw material used and on the pyrolysis conditions, where varying degrees of carbonization can produce a wide variety of biochars directing their application. The production of biochar does not require a fundamental scientific advance, the production technology is robust, simple and suitable for many regions of the world, but it becomes necessary to develop optimizations and economic evaluations to carry out large-scale production.

Concerning the oxidative atmosphere, it is easier to distinguish the different steps related to the decomposition of pseudo-components for low heating rates, thanks to the reduced overlapping of the peaks. Moreover, it must be highlighted the percentage of the residue at the end of the analysis, due to the presence of ash and char, respectively, in oxidative and inert atmospheres.

When the heating rate increased, the decomposition temperature range was moved towards higher values. In contradistinction to the oxidative atmosphere, the peak temperatures for the pseudo-

components could be directly assessed in inert conditions at low heating rates (2, 5, and 10 °C·min^{-1}). In this case, T_{p1} corresponds to the peak temperature of hemicellulose, while T_{p2} and T_{p3} to cellulose and lignin, respectively. The value of char peak temperature is not reported, due to the presence of a shoulder and not a real peak in the DTG chart. Nevertheless, for higher heating rates (15 and 20 °C·min^{-1}), the hemicellulose and cellulose peaks merged.

For a graphical interpretation of the contribution of the heating rate, the decomposition temperatures T_e, T_o and the temperature peaks T_{p1}, $T_{p2,}$ and T_{p3} are plotted in **Figure 4.9**.

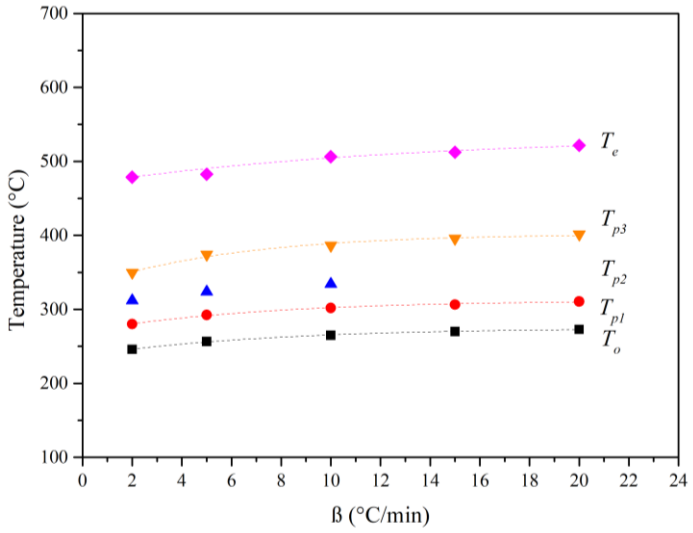

Figure 4.9: Evolution of the characteristic decomposition temperatures T_o, T_e, T_{p1}, $T_{p2,}$ and T_{p3} at β of 2, 5, 10, 15, 20 °C·min^{-1}.

The zero-decomposition temperature (ZDT) was calculated with **Equation 4.1**. All the obtained values are reported in **Table 4.6**, along with the fitting parameters and the regression coefficients for all the components. Given the decomposition of cellulose could not be determined at β of 15 and 20 °C·min^{-1} T_{p2} values were not included, and ZDT could not be calculated.

Table 4.5: Onset and endset degradation temperatures (T_o, T_e), peak temperature (T_p), and mass loss percentages for the different decomposition of components (Δm) obtained at β of 2, 5, 10, 15 and 20 °C·min^{-1}.

β (°C·min^{-1})	T_o	T_{po}	Δm_o	T_{p1}	Δm_1	T_{p2}	Δm_2	T_{p3}	Δm_3	T_e	R
	(°C)	(°C)	(%)	(°C)	(%)	(°C)	(%)	(°C)	(%)	(°C)	(%)
2	246	57±2	72	2802	35	312	11	350	10	479	22.2
5	257	70	72	2922	35	324	10	374	11	483	23.1
10	265±1	80±3	82	3022	34	334	12	386±3	14	506±1	20.5
15	270±1	90	72	3062	47	-	-	396±1	15	512	19.5
20	273	89	72	3112	48	-	-	401	14	522	20

Table 4.6: ZDT (β→0) values along with the fitting parameters and regression coefficient for T_o, T_e, T_{p1}, and T_{p3}

	ZDT(β → 0) (°C)	a	b	K	R^2
T_o	237	275±1	0.16	0.15	0.99
T_{p1}	271	312±2	0.15	0.16	0.99
T_{p3}	332	402±4	0.21	0.19	0.97
T_e	470	533±8	0.13	0.09	0.99

4.2.2. Modelling of the thermal decomposition

The deconvolution analysis was performed, employing the Lorentz function and five different peaks, corresponding to five pseudo-components of the biomass, were obtained. The **Figure 4.10** are shown the results of multi-peak fitting obtained for the DTG curves at 2, 5, 10, 15, and 20 °C·min^{-1}. For all of them, the correlation coefficients R^2 ranged between 0.97 and 0.99. Therefore, also in the case of an inert atmosphere, the developed analysis can explain rightly the characteristics of SCG thermal decomposition.

According to the data reported in the literature (Pinzi et al., 2020a), the release of the excess moisture takes place between 25 °C and 130-150 °C. The decomposition of the hemicellulose occurs in the 160-375 °C range, with a peak around 300 °C. Cellulose degrades at 270-400 °C, with a peak centred at 320-350 °C. Lignin has a wide degradation ranged between 300-320 °C and 460-470 °C. Finally, the degradation of remaining char occurs in the range of 420-530 °C although, as cited before, the decomposition is not complete at the end of the assay.

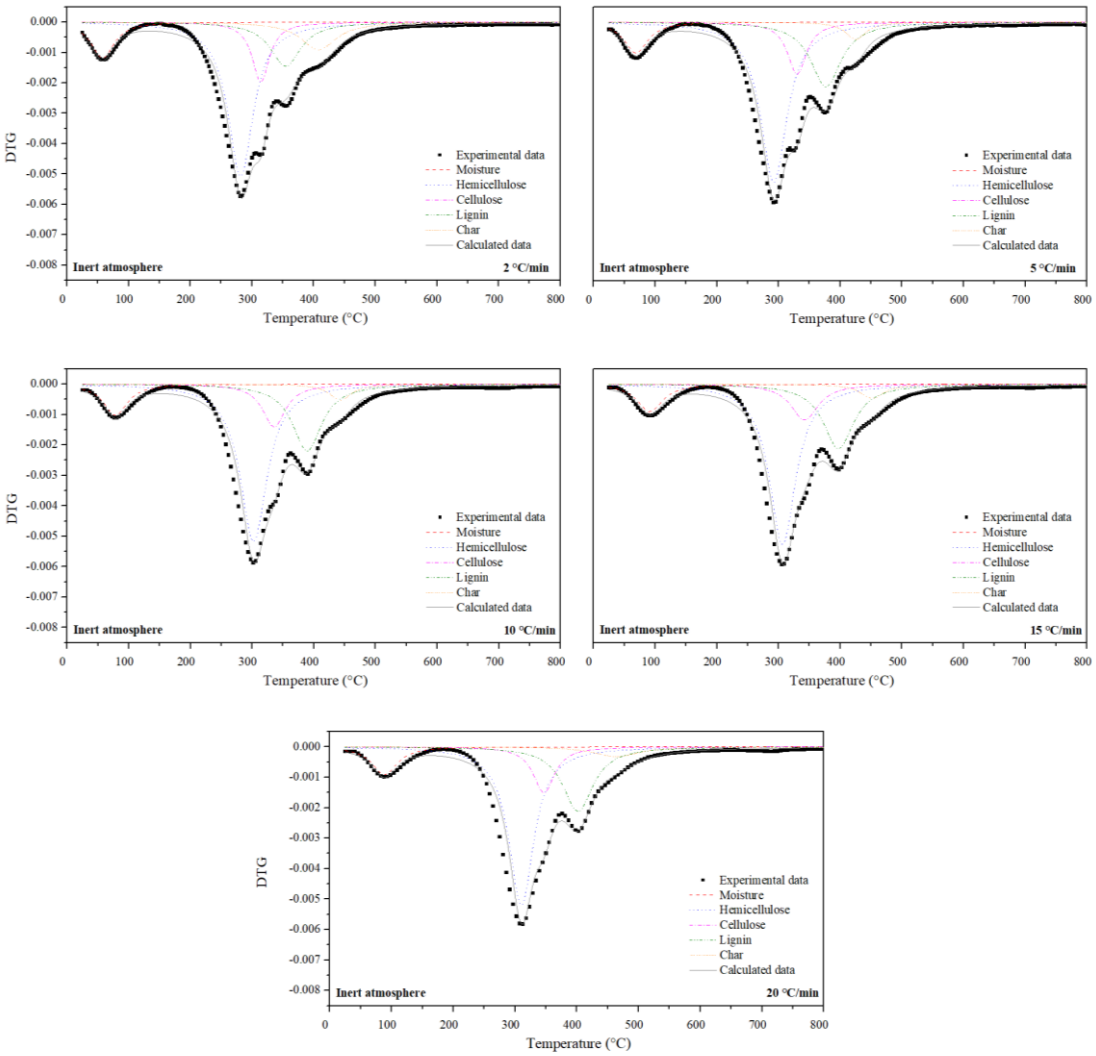

Figure 4.10: The Lorentz function deconvolution results of SCG under inert atmosphere at β of 2, 5, 10, 15, 20 °C·min^{-1}.

4.2.3. Kinetic analysis of the thermo-oxidative decomposition

In this section, the calculation of the kinetic triplet, obtained by the application of model-free kinetic analyses is reported. For this purpose, the results of a set of experimental tests at different heating rates (2, 5, 10, 15, and 20 °C·min^{-1}) were considered.

Activation Energy

The iso-conversional methods proposed by Friedman, FWO, and KAS, were applied. The conversion degree (α) for the kinetic analysis was selected in the range 0.2-0.8 to avoid initiation and termination reactions. The activation energy (E_a) at each conversion degree (α), was determined considering the slopes of the tendency lines, drawn for each set of points at different heating rates. **Figure 4.11** shows the linearized plots of hemicellulose, cellulose, and lignin for the three iso-conversional methods. Although activation energy for char could still be evaluated, its linearized plot revealed a low R^2 fitting and therefore it is was omitted in this section.

The fitting lines of the pseudo-components showed a fairly high degree of correlation (R^2) in the range of α from 0.2 to 0.8. For hemicellulose and lignin, R^2 is always between 0.96 and 0.99. Regarding cellulose, the situation is more complex. In the lower conversion degree (α) range of 0.2-0.3, R^2 is between 0.92 and 0.94, while for α in the range 0.35-0.8, R^2 is between 0.95 and 0.98. Therefore, this observation may be considered for the interpretation of results of the lower conversion degree. From the slopes of the linear fitting, the apparent activation energies were calculated and plotted in **Figure 4.12** as a function of the conversion degree.

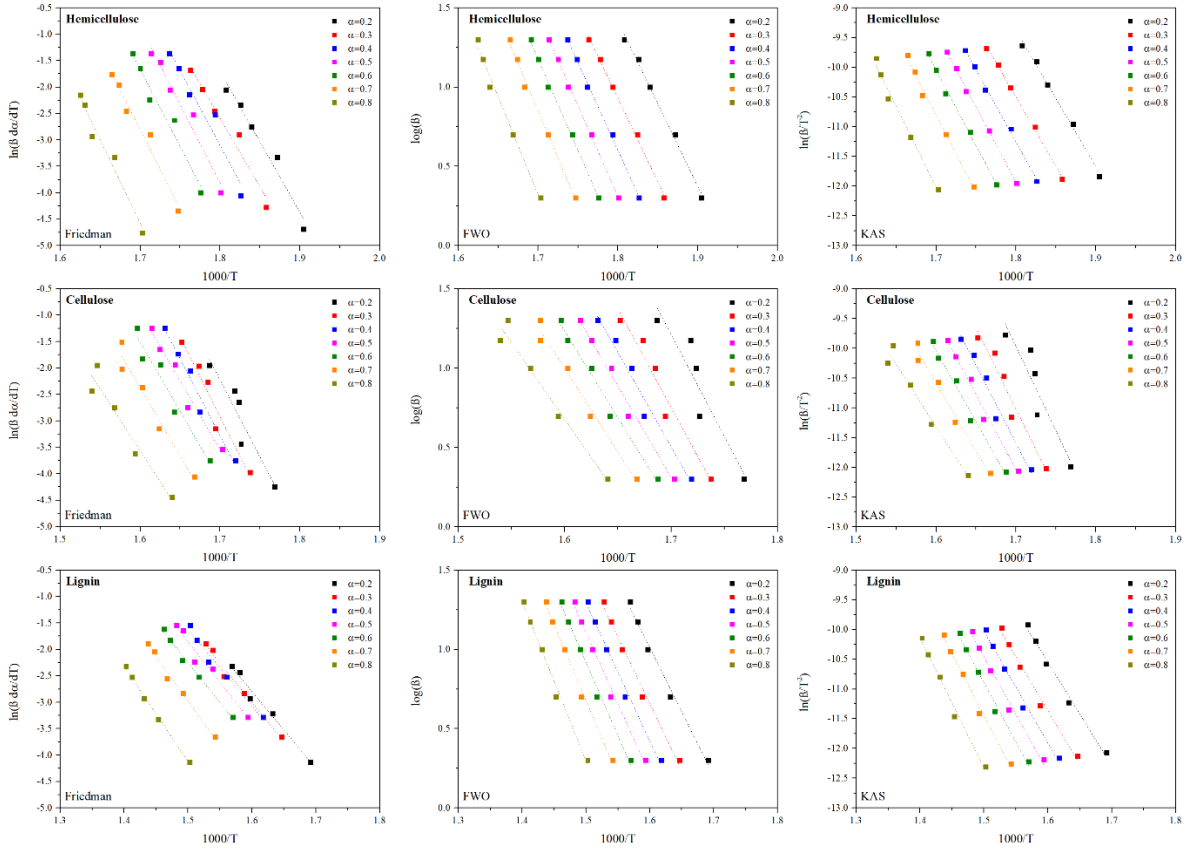

Figure 4.11: Friedman, FWO and KAS fitting plots of hemicellulose, cellulose and lignin for different α.

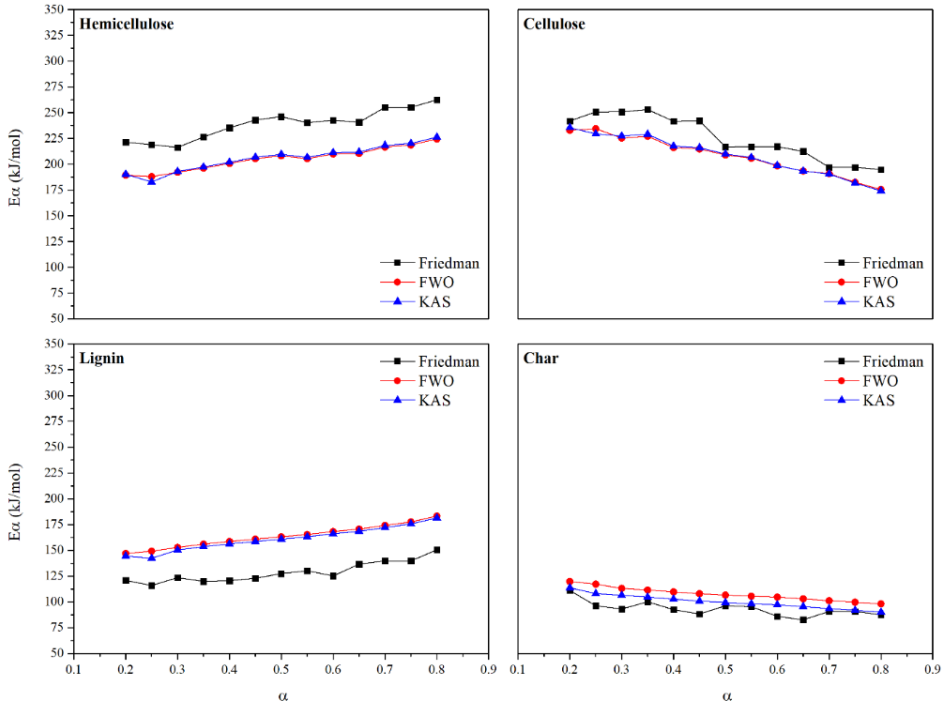

Figure 4.12: Evolution of apparent activation energy in the range of α from 0.2 to 0.8 calculated with different iso-conversional methods for the hemicellulose, cellulose, lignin, and char.

The calculated activation energy E_a as a function of α shows a quasi-constant behaviour. A slightly decreasing or increasing pattern was found with the increase of the conversation degree. For the cellulose and char, the activation energy was reduced, while for the hemicellulose and lignin the opposite situation occurs. As in the oxidative case, this phenomenon can be justified by the different chemical reactions that occur during the decomposition of a given pseudo-component, which vary when the decomposition advances, i.e. α increases.

The iso-conversional methods adopted for the calculation of E_a are dependent on the decomposition temperature ranges of the components, which are not constant with β. Indeed, observing the **Figure 4.12,** it's possible to see that for hemicellulose and lignin, the degradation temperature ranges become broader when decreasing the value of β, while for the cellulose and char, the degradation temperature ranges become narrower when decreasing the value of β. Considering that each of the tendency lines corresponds to a value of α, for the cellulose and char the slope decreases from α=0.2 to α=0.8, decreasing the value of E_a, while for the hemicellulose and lignin, the slope increases from α=0.2 to α=0.8, increasing the value of E_a. The **Table 4.7** collects the average values for the activation energy calculated in the range of conversion degree (α) from 0.2 to 0.8

Table 4.7: Average values for the activation energy (E_a) obtained with the different iso-conversional methods for hemicellulose, cellulose, lignin, and char.

Hemicellulose			Cellulose		
$E_{aFriedman}$ (kJ·mol^{-1})	E_{aFWO} (kJ·mol^{-1})	E_{aKAS} (kJ·mol^{-1})	$E_{aFriedman}$ (kJ·mol^{-1})	E_{aFWO} (kJ·mol^{-1})	E_{aKAS} (kJ·mol^{-1})
238.8	205	205.8	226	208	208
Lignin			**Char**		
$E_{aFriedman}$ (kJ·mol^{-1})	E_{aFWO} (kJ·mol^{-1})	E_{aKAS} (kJ·mol^{-1})	$E_{aFriedman}$ (kJ·mol-1)	E_{aFWO} (kJ·mol^{-1})	E_{aKAS} (kJ·mol^{-1})
128.7	163.6	161	150	156	152

Concerning the type of biomass considered, the values of E_a for the hemicellulose can vary from 115 kJ·mol^{-1} until 230 kJ·mol^{-1} (Pinzi et al., 2020a)(Moriana et al., 2014) (Amutio et al., 2012). In this study, a value of 220 kJ·mol^{-1} was found, which is within the range of the reported values for this pseudo-component. According to literature, the average value of E_a for the cellulose under pyrolytic conditions ranged between 195 kJ·mol^{-1} and 235 kJ·mol^{-1}, therefore, in compliance to the value obtained in this study, around 215 kJ·mol^{-1} (Amutio et al., 2011) (Şerbănescu, 2014). Furthermore, lignin revealed an average E_a of 150 kJ·mol^{-1}, aligned with different sources that confirm that the value of E_a for the lignin is between 130-160 kJ·mol^{-1} (Jiang et al., 2010) (Chen et al., 2017). Using these values of the activation energy, the kinetic function and the pre-exponential factor of the sample will be calculated.

Calculation of kinetic function and pre-exponential factor

The most appropriate kinetic mechanism for the pyrolysis of each component of the SCG under an inert atmosphere was graphically evaluated using reduced Master Plots. In **Figure 4.12** are plotted the experimental curves at a heating rate of 10 °C·min^{-1} with the theoretical *g(α)* curves for the typical decomposition mechanisms of biomass, reported in **Table 3.3**.

It was observed that all the reaction mechanisms were comparable to the curve of F_n type, with *n* equal to 1, 2, 3, and 4 or of D_3 type. In this case, a mechanism between the F_3 and F_4 type was considered for the hemicellulose, while for the lignin was selected the F_2 model. Additionally, for the char was evaluated the F_1 model. However, it was not possible to visually determine a single mechanism for the cellulose, because the experimental curve appears between F_3 and D_3 models. While for low conversion the thermal decomposition of cellulose would occur according to mechanism D_3, at higher conversion, the F_3 mechanism prevails. Finally, the D_3 type was selected according to the literature (López-González et al., 2013) (Pinzi et al., 2020b).

All the mechanisms considered comply with results reported in the literature, in which the mechanism of decomposition of lignocellulosic material components under inert conditions are identified as F_n or D_n mechanism, depending on the different materials (Pinzi et al., 2020b) (Moriana et al., 2014)(López-González et al., 2013).

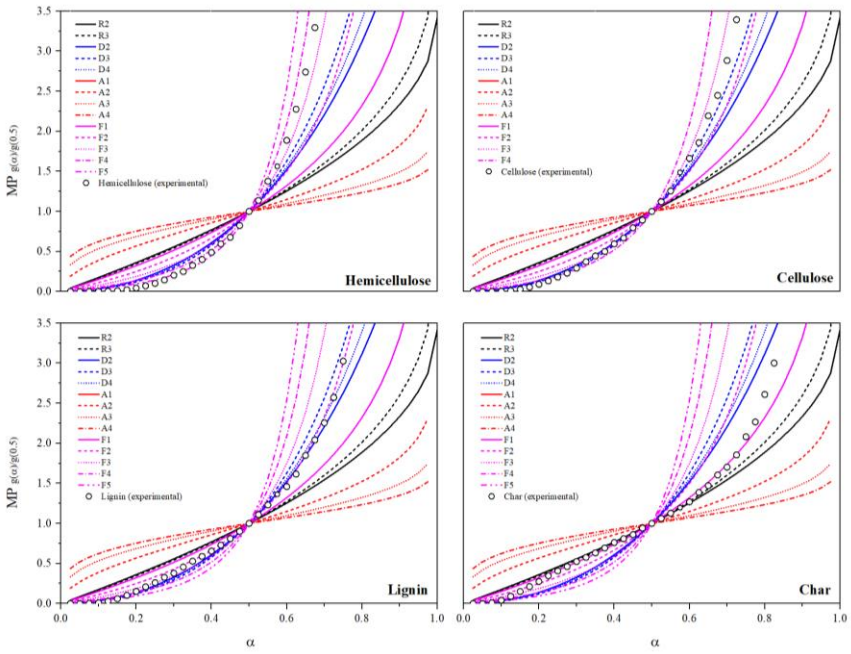

Figure 4.12: Normalised Master Plots in comparison to the decomposition process of hemicellulose, cellulose, lignin, and char at a heating rate of 10 °C·min^{-1}.

After the graphic evaluation of the most appropriate theoretical mechanism, the pre-exponential factor *A* was calculated, through the application of the Coast-Redfern equation (**equation 3.11**), and the optimal analytical *n* was estimated for each mechanism. **Figure 4.13** shows the plot of $\ln \frac{\beta\, g(\alpha)}{T^2}$ vs. $\frac{1000}{T}$ at each heating rate for hemicellulose, cellulose, lignin, and char. The straight lines in the Perez-Maqueda criterion charts confirm the good fitting of selected mechanisms (F_n and D_3).

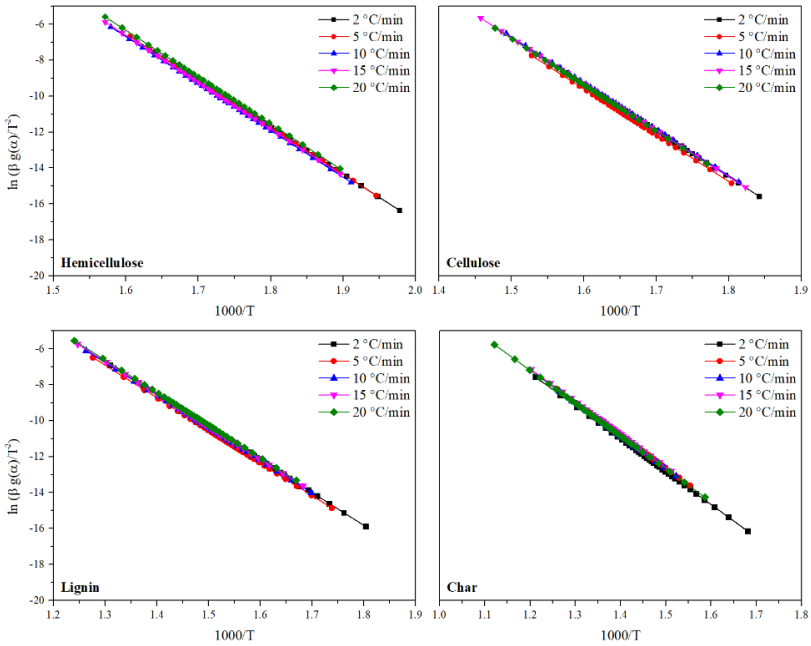

Figure 4.13: Application of the Perez-Maqueda *et al.* criterion for the simplified kinetic triplet of hemicellulose, cellulose, lignin, and char at a heating rate equal to 2, 5, 10, 20, 30 °C·min^{-1}.

In **Table 4.8** are reported all the values for the pre-exponential factor, calculated as an average between the A_β at the different heating rates, for the most appropriate mechanism of the reaction and the calculated analytical order of hemicellulose, cellulose, lignin, and char, under inert atmosphere. Moreover, *e* (%) is shown, which represents the average of absolute deviations from the mean in each set of $\ln(A_\beta)$.

Table 4.8: Frequency factor *A*, reaction mechanism, and reaction analytical order calculated applying Perez-Maqueda criterion for hemicellulose, cellulose, lignin, and char under oxidative atmosphere.

	Ln(A)	e (%)	n-MP	n
Hemicellulose	46	0.2	F3-F4	3.7
Cellulose	42	0.2	D3	-
Lignin	27	0.3	F2	2.3
Char	25	0.3	F1	1.8

The obtained results for the pre-exponential factor *A* related to the cellulose and hemicellulose are slightly lower for those obtained in other studies on the same components under inert atmosphere, while the *A* values for the lignin and char are higher (Moliner, Aguilar, et al., 2016).

However, also for the inert atmosphere, *A* is strictly related to the activation energy, and being that higher to the average value, slightly greater values for the pre-exponential factors were obtained.

The values of optimal analytical *n* calculated with the regression method, confirm the reaction mechanisms selected. Only the value of char appears slightly higher compared to the reduced Master plots. It may occur because the experimental curve plotted falls between the F_1 and R_3 models.

Overall, the obtained error (*e*) is very low, which validates the considered approach for assessing the kinetic triplet.

4.3. Kinetic triplet: thermo-oxidative versus thermal decomposition

Once separately evaluated both the thermo-oxidative and the thermal decomposition, this section highlights the similarities and differences of the kinetic results, obtained under both atmospheres. For this purpose, **Figure 4.13** shows the value of E_α for hemicellulose, cellulose, lignin, and char in the two atmospheres, as obtained from the average of the Friedman, FWO, and KAS methods.

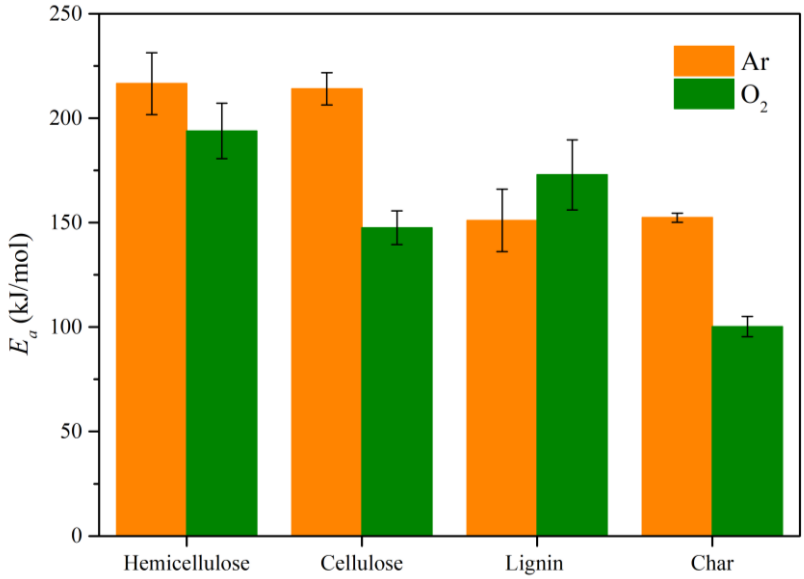

Figure 4.13: Average activation energy (E_α) of hemicellulose, cellulose, lignin, and char in oxidative and inert atmospheres.

The activation energy corresponds to the minimum amount of energy that must be provided to compounds to result in a chemical reaction. As expected, for all components, except for the lignin, the average value of E_α is higher in the inert atmosphere to the oxidative one. It occurs because, in the latter case, the oxidating agent reacts with the components, speeding up the degradation and decreasing the value of the energy barrier. As cited before, the decomposition process of lignin was difficult to adjust during deconvolution, especially at higher conversion, and also the values of the average calculated activation energy were similar, considering the deviation given by the different calculation methods.

Figure 4.14 displays the values of the frequency factor (A) in a logarithmic scale of hemicellulose, cellulose, lignin, and char in oxidative and inert atmospheres. The frequency factor is used to describe the rate of molecular collisions that occur in the chemical reaction. It is generally obtained experimentally to ensure that the parameters of the chemical reaction (temperature, activation energy, and constant rate) conform to the form of the Arrhenius equation. Given the strong dependence of A on the activation energy, an analogous pattern was found. In this regard, a higher frequency factor was determined for the decomposition process of the pseudo-components that occurred at lower temperatures.

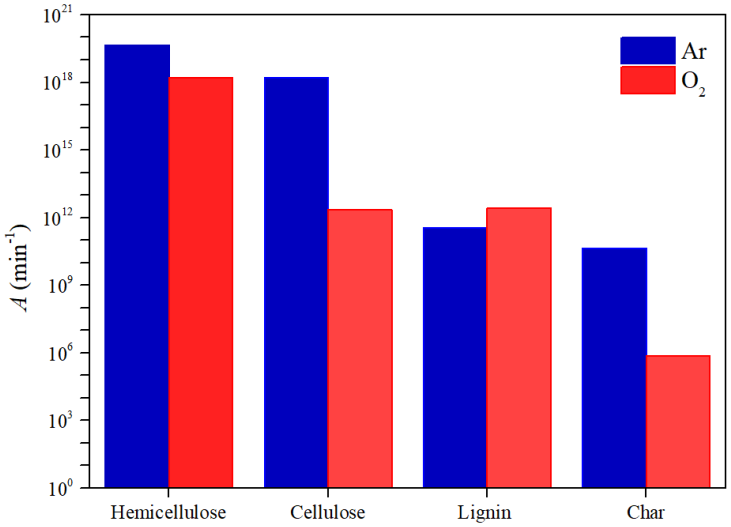

Figure 4.14: Frequency factor (*A*) of hemicellulose, cellulose, lignin, and char in oxidative and inert atmospheres.

Finally, **Table 4.9** presents the results for the *Ln(A)*, the reaction mechanism, and reaction analytical order calculated applying Perez-Maqueda criterion for hemicellulose, cellulose, lignin, and char under oxidative and inert atmospheres. Overall, similar decomposition mechanisms were found regardless of the atmosphere for hemicellulose (random nucleation), hemicellulose (three-dimensional diffusion), and lignin (random nucleation) pseudo-components.

Table 4.9: *Ln(A)*, reaction mechanism and reaction analytical order calculated applying Perez-Maqueda criterion for hemicellulose, cellulose, lignin, and char under oxidative and inert atmospheres.

	O_2			Ar		
	n-MP	***n***	***Ln(A)***	***n-MP***	***n***	***Ln(A)***
Hemicellulose	F4-F5	3.7	45.3	F3-F4	3.7	41.9
Cellulose	D3	-	41.9	D3	-	28.3
Lignin	F3-F4	3.6	26.6	F2	2.3	28.6
Char	A2	-	24.5	F1	1.8	13.5

5. Conclusions

The thermo-kinetical analysis carried out on the coffee spent grounds (SCG) in the inert and oxidative atmospheres to study their use as feedstock for energy production, has led to the following conclusions:

Under an inert atmosphere:

The coffee spent grounds tested at multiple heating rates exhibits a thermogravimetric thermogram with different overlapped peaks corresponding to the components of biomass.

Three main degradation stages are observed: Firstly, the devolatilization of humidity occurs, following by hemicellulose, cellulose, and a part of lignin decomposition. Finally, the degradation of the lignin and char takes place.

The zero decomposition temperature proves the thermal stability regardless of the heating rate.

Five peaks related to the biomass components are obtained and characterised with a detailed deconvolution analysis.

The degradation temperature ranges of the lignin result broader with respect to one of cellulose or hemicellulose, due to the complex degradation mechanisms of this component. The mass loss related to the remaining biochar is around 20%.

This biochar is a carbon-rich, porous solid generated in the process of partial thermochemical decomposition of biomass. It is the product of the elimination of volatile compounds present in the matter that consists of gases, oils, and tar.

Kinetic analyses revealed that: (I) Cellulose was described by a three-dimensional diffusion kinetic model ($D3$). It means that the gas atmosphere did not influence the reaction mechanism, which is, instead, controlled by the increase in the temperature and the diffusion of products. (II) Hemicellulose and lignin were described by random nucleation kinetic model (F_n). (III) Char was fit with a random nucleation kinetic model (F_n)

Under oxidative atmosphere:

Due to the coffee spent grounds composition is carbon and oxygen with low nitrogen and null sulphur content, with adequate control of the temperature, the thermo-oxidation products are mainly carbon dioxide and carbon monoxide. The generation of a low percentage of unwanted nitrogenous compounds makes this material attractive from the combustion perspective.

The thermogravimetric thermograms of coffee spent grounds, carried out at multiple heating rates, also show three degradation stages (i) the evaporation of humidity; (ii) the oxidation of hemicellulose, cellulose, and lignin; (iii) decomposition of the rest of lignin and char. The thermo-oxidative decomposition of the remaining char following until obtaining only ash as residue.

Kinetic analyses prove that cellulose and hemicellulose were described by the same three-dimensional diffusion kinetic model ($D3$) and random nucleation kinetic model (F_n). The order of reaction for both components results higher in the oxidative atmosphere than the inert one. In these cases, the presence of the oxidation agent allows to speed up the reaction. The activation energy in oxidative is lower than in an inert atmosphere due to the contribution of the presence of oxygen, especially in the thermo-oxidation of hemicellulose, cellulose, and char.

Overall, according to the low ash yield and relatively high calorific value, the environmental benefit, and the kinetic results obtained, this kind of biomass, derived from the coffee production process, may be promoted as a renewable source of energy.

6. References

Al-Hamamre, Z., Foerster, S., Hartmann, F., Kröger, M., & Kaltschmitt, M. (2012). Oil extracted from spent coffee grounds as a renewable source for fatty acid methyl ester manufacturing. *Fuel*, *96*(x), 70–76. https://doi.org/10.1016/j.fuel.2012.01.023

Allesina, G., Pedrazzi, S., Allegretti, F., & Tartarini, P. (2017). Spent coffee grounds as heat source for coffee roasting plants: Experimental validation and case study. *Applied Thermal Engineering*, *126*, 730–736. https://doi.org/10.1016/j.applthermaleng.2017.07.202

Amutio, M., Lopez, G., Aguado, R., Artetxe, M., Bilbao, J., & Olazar, M. (2011). Effect of vacuum on lignocellulosic biomass flash pyrolysis in a conical spouted bed reactor. *Energy and Fuels*, *25*(9), 3950–3960. https://doi.org/10.1021/ef200712h

Amutio, M., Lopez, G., Aguado, R., Artetxe, M., Bilbao, J., & Olazar, M. (2012). Kinetic study of lignocellulosic biomass oxidative pyrolysis. *Fuel*, *95*, 305–311. https://doi.org/10.1016/j.fuel.2011.10.008

Arulrajah, A., Maghoolpilehrood, F., Disfani, M. M., & Horpibulsuk, S. (2014). Spent coffee grounds as a non-structural embankment fill material: Engineering and environmental considerations. *Journal of Cleaner Production*, *72*, 181–186. https://doi.org/10.1016/j.jclepro.2014.03.010

Ballesteros, L. F., Teixeira, J. A., & Mussatto, S. I. (2014). Chemical, Functional, and Structural Properties of Spent Coffee Grounds and Coffee Silverskin. *Food and Bioprocess Technology*, *7*(12), 3493–3503. https://doi.org/10.1007/s11947-014-1349-z

Basu, P. (2013). Biomass Gasification, Pyrolysis and Torrefaction: Practical Design and Theory. In *Biomass Gasification, Pyrolysis and Torrefaction: Practical Design and Theory*. https://doi.org/10.1016/C2011-0-07564-6

Bedmutha, R., Booker, C. J., Ferrante, L., Briens, C., Berruti, F., Yeung, K. K. C., Scott, I., & Conn, K. (2011). Insecticidal and bactericidal characteristics of the bio-oil from the fast pyrolysis of coffee grounds. *Journal of Analytical and Applied Pyrolysis*, *90*(2), 224–231. https://doi.org/10.1016/j.jaap.2010.12.011

Caetano, N. S., Caldeira, D., Martins, A. A., & Mata, T. M. (2017). Valorisation of Spent Coffee Grounds: Production of Biodiesel via Enzymatic Catalysis with Ethanol and a Co-solvent. *Waste and Biomass Valorization*, *8*(6), 1981–1994. https://doi.org/10.1007/s12649-016-9790-z

Caetano, Nídia S., Silva, V. F. M., Melo, A. C., Martins, A. A., & Mata, T. M. (2014). Spent coffee grounds for biodiesel production and other applications. *Clean Technologies and Environmental Policy*, *16*(7), 1423–1430. https://doi.org/10.1007/s10098-014-0773-0

Caetano, Nídia S., Silvaa, V. F. M., & Mata, T. M. (2012). Valorization of coffee grounds for biodiesel production. *Chemical Engineering Transactions*, *26*(January), 267–272. https://doi.org/10.3303/CET1226045

Campos-Vega, R., Loarca-Piña, G., Vergara-Castañeda, H. A., & Dave Oomah, B. (2015). Spent coffee grounds: A review on current research and future prospects. *Trends in Food Science and Technology*, *45*(1), 24–36. https://doi.org/10.1016/j.tifs.2015.04.012

Chen, T., Li, L., Zhao, R., & Wu, J. (2017). Pyrolysis kinetic analysis of the three pseudocomponents of biomass–cellulose, hemicellulose and lignin: Sinusoidally modulated temperature method. *Journal of Thermal Analysis and Calorimetry*, *128*(3), 1825–1832. https://doi.org/10.1007/s10973-016-6040-3

Coats. A.W., Redfern, J. . (1964). *Kinetic Parameters from Thermogravimetric Data*. *201*, 68–69.

Confederación Internacional para el Análisis Térmico I.C.T.A Internacional Commitee Thermal Analysis. (n.d.).

Criado, J. M., Málek, J., & Ortega, A. (1989). Applicability of the master plots in kinetic analysis of non-isothermal data. *Thermochimica Acta*, *147*(2), 377–385. https://doi.org/10.1016/0040-6031(89)85192-5

Daramola, M. O., & Ayeni, A. O. (2020). *Valorization of Biomass to Value-Added Commodities Current Trends, Challenges, and Future Prospects.*

Ding, Y., Huang, B., Wu, C., He, Q., & Lu, K. (2019). Kinetic model and parameters study of lignocellulosic biomass oxidative pyrolysis. *Energy*, *181*, 11–17. https://doi.org/10.1016/j.energy.2019.05.148

Döhlert, P., Weidauer, M., & Enthaler, S. (2016). Spent coffee ground as source for hydrocarbon fuels. *Journal of Energy Chemistry*, *25*(1), 146–152. https://doi.org/10.1016/j.jechem.2015.11.012

Dunmade, I. (2013). Sustainability Issues in Innovative Waste Reduction Technology Adoption and Assimilation. *International Journal of Environmental Protection and Policy*, *1*(4), 59. https://doi.org/10.11648/j.ijepp.20130104.13

Dunmade, I. S., Oyedepo, S., Fayomi, O., & Udo, M. (2019). Government Policies and Engineers' Roles in Facilitating Nigeria's Transition to Circular Economy. *Journal of Physics: Conference Series*, *1378*(2). https://doi.org/10.1088/1742-6596/1378/2/022097

Esquivel, P., & Jiménez, V. M. (2012). Functional properties of coffee and coffee by-products. *Food Research International*, *46*(2), 488–495. https://doi.org/10.1016/j.foodres.2011.05.028

Foukis, A., Gkini, O. A., Stergiou, P. Y., Sakkas, V. A., Dima, A., Boura, K., Koutinas, A., & Papamichael, E. M. (2017). Sustainable production of a new generation biofuel by lipase-catalyzed esterification of fatty acids from liquid industrial waste biomass. *Bioresource Technology*, *238*, 122–128. https://doi.org/10.1016/j.biortech.2017.04.028

Friedman, H. L. (2007). Kinetics of thermal degradation of char-forming plastics from thermogravimetry. Application to a phenolic plastic. *Journal of Polymer Science Part C: Polymer Symposia*, *6*(1), 183–195. https://doi.org/10.1002/polc.5070060121

Greus, A. R., Domingo, F. V., & Rodrigo, L. C. (2008). *Thermal characterisation of polymeric materials*.

Hornung, A. (2014). Transformation of Biomass [School of Chemical Engineering College of Engineering and Physical Sciences University of Birmingham, UK]. In *© 2014 John Wiley & Sons, Ltd*. https://doi.org/10.1002/9781118693643

Isikgor, F. H., & Becer, C. R. (2015). Lignocellulosic biomass: a sustainable platform for the production of bio-based chemicals and polymers. *Polymer Chemistry*, *6*(25), 4497–4559. https://doi.org/10.1039/c5py00263j

Jiang, G., Nowakowski, D. J., & Bridgwater, A. V. (2010). A systematic study of the kinetics of lignin pyrolysis. *Thermochimica Acta*, *498*(1–2), 61–66. https://doi.org/10.1016/j.tca.2009.10.003

Khawam, A., & Flanagan, D. R. (2006). Solid-state kinetic models: Basics and mathematical fundamentals. *Journal of Physical Chemistry B*, *110*(35), 17315–17328. https://doi.org/10.1021/jp062746a

Kok, M. V., & Özgür, E. (2013). Thermal analysis and kinetics of biomass samples. *Fuel Processing Technology*, *106*, 739–743. https://doi.org/10.1016/j.fuproc.2012.10.010

Kongkaew, N., Pruksakit, W., & Patumsawad, S. (2015). Thermogravimetric Kinetic Analysis of the

Pyrolysis of Rice Straw. In *Energy Procedia* (Vol. 79). Elsevier B.V. https://doi.org/10.1016/j.egypro.2015.11.552

Lascano, D., Garcia-Garcia, D., Rojas-Lema, S., Quiles-Carrillo, L., Balart, R., & Boronat, T. (2020). Manufacturing and characterization of green composites with partially biobased epoxy resin and flaxseed flour wastes. *Applied Sciences (Switzerland)*, *10*(11). https://doi.org/10.3390/app10113688

Lee, X. J., Ong, H. C., Gao, W., Ok, Y. S., Chen, W. H., Goh, B. H. H., & Chong, C. T. (2021). Solid biofuel production from spent coffee ground wastes: Process optimisation, characterisation and kinetic studies. *Fuel*, *292*(February), 120309. https://doi.org/10.1016/j.fuel.2021.120309

López-González, D., Fernandez-Lopez, M., Valverde, J. L., & Sanchez-Silva, L. (2013). Thermogravimetric-mass spectrometric analysis on combustion of lignocellulosic biomass. *Bioresource Technology*, *143*, 562–574. https://doi.org/10.1016/j.biortech.2013.06.052

Mata, T. M., Martins, A. A., & Caetano, N. S. (2018). Bio-refinery approach for spent coffee grounds valorization. *Bioresource Technology*, *247*(July 2017), 1077–1084. https://doi.org/10.1016/j.biortech.2017.09.106

McKendry, P. (2002). Energy production from biomass (part 1): Overview of biomass. *Bioresource Technology*, *83*(1), 37–46. https://doi.org/10.1016/S0960-8524(01)00118-3

Menczel, J. D., & Prime, R. B. (2008). Thermal Analysis of Polymers: Fundamentals and Applications. In *Thermal Analysis of Polymers: Fundamentals and Applications*. https://doi.org/10.1002/9780470423837

Mohan, D., Pittman, C. U., & Steele, P. H. (2006). Pyrolysis of wood/biomass for bio-oil: A critical review. *Energy and Fuels*, *20*(3), 848–889. https://doi.org/10.1021/ef0502397

Moliner, C., Aguilar, K., Bosio, B., Arato, E., & Ribes, A. (2016). Thermo-oxidative characterisation of the residues from persimmon harvest for its use in energy recovery processes. *Fuel Processing Technology*, *152*, 421–429. https://doi.org/10.1016/j.fuproc.2016.07.008

Moliner, C., Bosio, B., Arato, E., & Ribes, A. (2016). Thermal and thermo-oxidative characterisation of rice straw for its use in energy valorisation processes. *Fuel*, *180*, 71–79. https://doi.org/10.1016/j.fuel.2016.04.021

Moriana, R., Zhang, Y., Mischnick, P., Li, J., & Ek, M. (2014). Thermal degradation behavior and kinetic analysis of spruce glucomannan and its methylated derivatives. *Carbohydrate Polymers*, *106*(1), 60–70. https://doi.org/10.1016/j.carbpol.2014.01.086

Murthy, P. S., Naidu, M. M., & Srinivas, P. (2009). Production of α-amylase under solid-state fermentation utilizing coffee waste. *Journal of Chemical Technology and Biotechnology*, *84*(8), 1246–1249. https://doi.org/10.1002/jctb.2142

Mussatto, S. I., Ballesteros, L. F., Martins, S., & Teixeira, J. A. (2011). Extraction of antioxidant phenolic compounds from spent coffee grounds. *Separation and Purification Technology*, *83*(1), 173–179. https://doi.org/10.1016/j.seppur.2011.09.036

Mussatto, S. I., Carneiro, L. M., Silva, J. P. A., Roberto, I. C., & Teixeira, J. A. (2011). A study on chemical constituents and sugars extraction from spent coffee grounds. *Carbohydrate Polymers*, *83*(2), 368–374. https://doi.org/10.1016/j.carbpol.2010.07.063

Mussatto, S. I., Machado, E. M. S., Martins, S., & Teixeira, J. A. (2011). Production, Composition, and Application of Coffee and Its Industrial Residues. *Food and Bioprocess Technology*, *4*(5), 661–672. https://doi.org/10.1007/s11947-011-0565-z

Nunes, L. J. R., De Oliveira Matias, J. C., & Da Silva Catalão, J. P. (2018). Physical Pretreatment of Biomass. In *Torrefaction of Biomass for Energy Applications*. https://doi.org/10.1016/b978-0-12-809462-4.00002-x

Obruca, S., Benesova, P., Kucera, D., Petrik, S., & Marova, I. (2015). Biotechnological conversion of spent coffee grounds into polyhydroxyalkanoates and carotenoids. *New Biotechnology*, *32*(6), 569–574. https://doi.org/10.1016/j.nbt.2015.02.008

Ozawa, T. (1965). A New Method of Analyzing Thermogravimetric Data. *Bulletin of the Chemical Society of Japan*, *38*(11), 1881–1886. https://doi.org/10.1246/bcsj.38.1881

Pérez-Maqueda, L. A., & Criado, J. M. (2000). Accuracy of Senum and Yang's approximations to the Arrhenius integral. *Journal of Thermal Analysis and Calorimetry*, *60*(3), 909–915. https://doi.org/10.1023/A:1010115926340

Pérez-Maqueda, L. A., Criado, J. M., Gotor, F. J., & Málek, J. (2002). Advantages of combined kinetic analysis of experimental data obtained under any heating profile. *Journal of Physical Chemistry A*, *106*(12), 2862–2868. https://doi.org/10.1021/jp012246b

Pinzi, S., Buratti, C., Bartocci, P., Marseglia, G., Fantozzi, F., & Barbanera, M. (2020a). A simplified method for kinetic modeling of coffee silver skin pyrolysis by coupling pseudo-components peaks deconvolution analysis and model free-isoconversional methods. *Fuel*, *278*(May), 118260. https://doi.org/10.1016/j.fuel.2020.118260

Pinzi, S., Buratti, C., Bartocci, P., Marseglia, G., Fantozzi, F., & Barbanera, M. (2020b). A simplified method for kinetic modeling of coffee silver skin pyrolysis by coupling pseudo-components peaks deconvolution analysis and model free-isoconversional methods. *Fuel*, *278*(April), 118260. https://doi.org/10.1016/j.fuel.2020.118260

Primaz, C. T. (2018). *Valorização de resíduos agroindustriais de café e algodão para produção de bio-óleo e biochar.* 1–235.

Prins, M. J. (2005). Thermodynamic analysis of biomass gasification and torrefaction. In *Library* (Issue 2005). https://doi.org/10.6100/IR583729

Rego, F., Soares Dias, A. P., Casquilho, M., Rosa, F. C., & Rodrigues, A. (2019). Fast determination of lignocellulosic composition of poplar biomass by thermogravimetry. *Biomass and Bioenergy*, *122*(March 2018), 375–380. https://doi.org/10.1016/j.biombioe.2019.01.037

Santos, C., Fonseca, J., Aires, A., Coutinho, J., & Trindade, H. (2017). Effect of different rates of spent coffee grounds (SCG) on composting process, gaseous emissions and quality of end-product. *Waste Management*, *59*, 37–47. https://doi.org/10.1016/j.wasman.2016.10.020

Santos, C. M., de Oliveira, L. S., Alves Rocha, E. P., & Franca, A. S. (2020). Thermal conversion of defective coffee beans for energy purposes: Characterization and kinetic modeling. *Renewable Energy*, *147*, 1275–1291. https://doi.org/10.1016/j.renene.2019.09.052

Şerbănescu, C. (2014). Kinetic analysis of cellulose pyrolysis: A short review. *Chemical Papers*, *68*(7), 847–860. https://doi.org/10.2478/s11696-013-0529-z

Stylianou, M., Agapiou, A., Omirou, M., Vyrides, I., Ioannides, I. M., Maratheftis, G., & Fasoula, D. (2018). Converting environmental risks to benefits by using spent coffee grounds (SCG) as a valuable resource. *Environmental Science and Pollution Research*, *25*(36), 35776–35790. https://doi.org/10.1007/s11356-018-2359-6

Tun, M. M., Raclavská, H., Juchelková, D., Růžičková, J., Šafář, M., Štrbová, K., & Gikas, P. (2020). Spent coffee ground as renewable energy source: Evaluation of the drying processes. *Journal of*

Environmental Management, *275*(July). https://doi.org/10.1016/j.jenvman.2020.111204

Tuntiwiwattanapun, N., Usapein, P., & Tongcumpou, C. (2017). The energy usage and environmental impact assessment of spent coffee grounds biodiesel production by an in-situ transesterification process. *Energy for Sustainable Development*, *40*, 50–58. https://doi.org/10.1016/j.esd.2017.07.002

Vol, P. L., Method, D., The, F. O. R., Of, D., Energy, A., & The, T. D. (1988). The land molluscs of the Krakatau Islands, Indonesia. *Philosophical Transactions of the Royal Society of London. B, Biological Sciences*, *322*(1211), 379–400. https://doi.org/10.1098/rstb.1988.0133

Volf, I., Ignat, I., Neamtu, M., & Popa, V. I. (2014). Thermal stability, antioxidant activity, and photo-oxidation of natural polyphenols. *Chemical Papers*, *68*(1), 121–129. https://doi.org/10.2478/s11696-013-0417-6

Yaman, S. (2004). Pyrolysis of biomass to produce fuels and chemical feedstocks. *Energy Conversion and Management*, *45*(5), 651–671. https://doi.org/10.1016/S0196-8904(03)00177-8

Yamane, K., Kono, M., Fukunaga, T., Iwai, K., Sekine, R., Watanabe, Y., & Iijima, M. (2014). Field evaluation of coffee grounds application for crop growth enhancement, weed control, and soil improvement. *Plant Production Science*, *17*(1), 93–102. https://doi.org/10.1626/pps.17.93

ECONOMIC STUDY

1. Detailed budget

The detailed budget of the current work is divided into four different sections: the workforce, the budget associated with the equipment and tools, the materials and reagents, and the supplementary costs. The prices applied to correspond to the current costs and are reported without the Value Added Tax (VAT), which is applied at the end of this chapter. The euro (€) is the monetary unit used to calculate the budget.

1.1. Workforce

In this section are analysed the costs related to the staff employed to carry out the project. The staff is composed of a Chemical Engineer, and a Doctor in Industrial Engineering and Production, and Doctor in Chemistry, the supervisors of the project. The costs are valued in a fraction of time, applying the price in €/h. **Table 1** shows the project's workforce budget.

Table 1: Assumption of workforce

Workforce					
Ref	**Un**	**Description**	**Price (€)**	**Quantity**	**COST (€)**
O1	h	Chemical Engineering student	19.99	360	7196.40
O2	h	Doctor in Chemical Engineering (Supervisor of the project)	31.45	25	786.25
O3	h	Doctor in Chemistry (Supervisor of the project)	51.40	25	1285.00
				TOTAL	**9267.65**

1.2. Equipment and tools

In this section are shown the depreciable costs of the equipment and tools, already available and used for this work. For the equipment presented in **Table 2**, an amortisation period of 10 years was estimated, while for the tools 6 years was considered. The price is calculated for the duration of the project, which is approximately 3 months.

Table 2: Assumption for amortisation of equipment and tools.

Equipment and tools						
Ref	**Un**	**Description**	**Acquisition price (€)**	**Amortization price(€·year^{-1})**	**Quantity**	**COST (€)**
E1	year	Thermal-Gravimetric Anlysis equipment (TGA). Mettler Toledo/STDA 851	25000.00	2500.00	0.25	625.00
E2	year	PC	900.00	150.00	0.25	37.50
					TOTAL	**662.50**

1.3. Materials and reagents

This group includes all non-depreciable materials used to carry out the work. Therefore, the prices applied are the acquisition ones. Reagents and auxiliary materials are reported in **Table 3** and **4**, respectively.

Table 3: Assumption for reagents.

Reagents					
Ref	**Un**	**Description**	**Acquisition price (€)**	**Quantity**	**COST(€)**
R1	Bullet	Argon	75.00	0.5	37.50
R2	Bullet	Oxygen	75.00	0.5	37.50
				TOTAL	**75.00**

Table 4: Assumption for auxiliary materials.

Auxiliary materials					
Ref	**Un**	**Description**	**Acquisition price (€)**	**Quantity**	**COST(€)**
M1	Un	Mettler Toledo Alumina Crucibles 70 µL	30.10	34	1023.40
				TOTAL	**1023.40**

1.4 Supplementary costs

In this section, all the costs related to office supplies, software licenses, and the consumption of electricity needed for the project are shown in **Table 5**.

Table 5: Assumption for the supplementary costs.

Supplementary costs	
Concept	**COSTS (€)**
Other laboratory materials	100.00
License STAR Mettler Toledo	1500.00
Electricity consumption	150.00
TOTAL	**1750.00**

2. Total budget

This section it's presents a sum of all partial assumptions, realized in the previous sections, to obtain the final budget, which is shown in **Table 6**.

Table 6: Total budget.

Chapter	COSTS (€)
Workforce	9267.65
Equipment and tools	662.50
Reagents	75.00
Auxiliary materials	1023.40
Supplementary costs	1750.00
Material execution budget	**12778.55**
VAT 21%	2683.50
Contract execution budget	**15462.10**

The final budget to realize this project of the Master Thesis is FIFTYTEEN THOUSAND FOUR HUNDRED SIXTY-TWO POINT TEN

In this work, the workforce is not considered given that it is contextualised in the academic framework as a Final Master Thesis. Therefore, the real budget is reported in **Table 7.**

Table 7: Real budget.

Chapter	COSTS (€)
Equipment and tools	662.50
Reagents	75.00
Auxiliary materials	1023.40
Supplementary costs	1750.00
Material execution budget	**3510.90**
VAT 21%	737.29
Contract execution budget	**4248.20**

The real budget is FOUR THOUSAND TWO HUNDRED FORTY-EIGHT POINT TWENTY.